

OAK RIDGE NATIONAL LABORATORY LIBRARIES



3 4456 0555435 2

ORNL/TM-7567

ornl

OAK
RIDGE
NATIONAL
LABORATORY

UNION
CARBIDE

Theoretical Characterization of a Dual Purpose Gamma Thermometer

T. J. Burns
J. O. Johnson

OAK RIDGE NATIONAL LABORATORY

CENTRAL RESEARCH LIBRARY

CIRCULATION SECTION

4500N ROOM 175

LIBRARY LOAN COPY

DO NOT TRANSFER TO ANOTHER PERSON

If you wish someone else to see this
report, send in name with report and
the library will arrange a loan.

JCN 7963 3 9 77

OPERATED BY
UNION CARBIDE CORPORATION
FOR THE UNITED STATES
DEPARTMENT OF ENERGY



This report was prepared as an account of work sponsored by an agency of the United States Government. Neither the United States Government nor any agency thereof, nor any of their employees, makes any warranty, express or implied, or assumes any legal liability or responsibility for the accuracy, completeness, or usefulness of any information, apparatus, product, or process disclosed, or represents that its use would not infringe privately owned rights. Reference herein to any specific commercial product, process, or service by trade name, trademark, manufacturer, or otherwise, does not necessarily constitute or imply its endorsement, recommendation, or favoring by the United States Government or any agency thereof. The views and opinions of authors expressed herein do not necessarily state or reflect those of the United States Government or any agency thereof.

ORNL/TM-7567

Contract No. W-7405-eng-26
Engineering Physics Division

THEORETICAL CHARACTERIZATION OF A DUAL PURPOSE
GAMMA THERMOMETER

T. J. Burns
J. O. Johnson*

Date Published - January 1981

NOTICE This document contains information of a preliminary nature.
It is subject to revision or correction and therefore does not represent a
final report.

*University of Tennessee, Department of Nuclear Engineering,
Knoxville, Tennessee 37916

OAK RIDGE NATIONAL LABORATORY
Oak Ridge, Tennessee 37830
operated by
UNION CARBIDE CORPORATION
for the
DEPARTMENT OF ENERGY

OAK RIDGE NATIONAL LABORATORY LIBRARIES



3 4456 0555435 2



TABLE OF CONTENTS

ACKNOWLEDGEMENTS	v
ABSTRACTvii
I. INTRODUCTION	1
1.0. Background	1
1.1. Technical Summary of the Proposed Gamma Thermometer. . .	3
1.1.1. Physical Description	3
1.1.2. Use of the Gamma Thermometer as a Power Level Monitor.	3
1.1.3. Use of the Gamma Thermometer as a Fluid Level Indicator.	5
1.1.4. Objectives and Scope of Investigation.	5
II. THEORETICAL ANALYSIS OF THE DUAL PURPOSE GAMMA THERMOMETER . .	7
III. RADIATION TRANSPORT ANALYSIS	12
IV. THERMAL HYDRAULIC ANALYSIS	32
V. CONCLUSIONS AND RECOMMENDATIONS.	43
REFERENCES	47
APPENDIX	49



ACKNOWLEDGEMENTS

The authors would like to express their sincere appreciation to R. L. Childs, M. L. Williams and W. A. Rhoades for their consultation in solving the problems which arose in the radiation transport analysis.

The authors would also like to acknowledge Katie Lawhorn and LaWanda Klobe who have patiently contributed their skills and talents toward the final preparation of this document.



ABSTRACT

A preliminary analytical and computational study was performed to investigate the potential of a modified gamma thermometer (GT) as both a power level monitor and fluid level monitor for a Pressurized Water Reactor (PWR). This study consisted of two fundamental parts: a radiation field characterization and a thermal-hydraulics analysis.

The radiation transport analysis was performed to determine the volumetric heat source within the GT due to gamma heating. Both fission product decay gammas and neutron induced gammas were included in the analysis. Further, a sensitivity analysis was performed to characterize the origin of the neutron induced gammas (by neutron reaction and material) contributing to the volumetric heat source. Utilizing this source, a series of thermal hydraulic calculations was performed to model certain reactor transients of interest (i.e., reactor scram, LOCA, etc.), in order to characterize the gamma thermometer response relative to power level monitoring and fluid level indication.

The results of this preliminary study confirm the feasibility of utilizing the GT as a dual function (power level and fluid level) measurement device. The study also indicates that each function can be accomplished virtually independent of the other. Therefore, the results provide encouragement and incentive to pursue the GT as a viable nuclear instrument.



I. INTRODUCTION

1.0. Background

The need for measuring the local power generation in a Light Water Reactor (LWR) is typically mandated by the material limitations of the reactor's fuel assemblies (i.e., cladding burnout, critical heat flux, etc.). Typically, the local power generation rate is inferred from measurements of the thermal neutron flux via self-powered neutron detectors (SPND's) or fission chambers. Recently, however, there has been an increased interest in the use of an alternative instrument, the gamma thermometer (GT), for the measurement of the local power generation rate.^{1,2} The gamma thermometer, originally developed for heavy-water reactors, has been proposed as a replacement for the SPND's currently utilized in LWR's. As an indication of the utility interest in these devices, Duke Power is currently involved in an experimental program utilizing gamma thermometers in one of the Oconee reactors. Further, the Tennessee Valley Authority (TVA) has initiated a \$400,000 program to passively irradiate gamma thermometers in the Oak Ridge National Laboratories Research Reactor (ORNL-ORR) in order to assess the calibration versus irradiation characteristics.

The increased interest in the gamma thermometer is related to the spatial variation of the thermal neutron and gamma fluxes within a LWR fuel assembly. The thermal neutron flux exhibits a large amount of structure as a function of position within the fuel assembly; whereas, the gamma flux shows very little structure. This behavior is depicted graphically in Fig. 1, which represents the spatial distribution of the thermal neutron flux and total gamma flux (both normalized to the centerline flux) for a one-dimensional XSDRNPM³ cell calculation. Since the existing SPND's are located in the water gaps, slight changes in the detector locations (e.g., through vibrations) as well as variations in the gap size, cladding thickness, etc. cause significant changes in the detector signal. To allow for uncertainties inherent in geometry, enrichment, etc., the operating limits of the reactor are typically set somewhat below the nominal design limits. Due to the slight deviation in the gamma flux

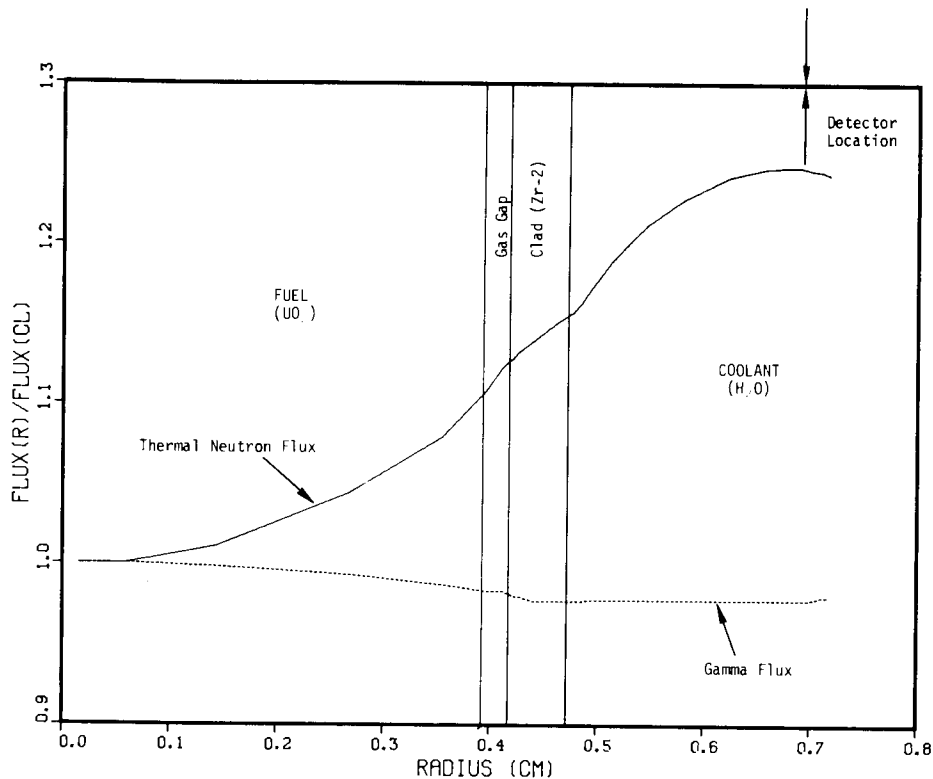


Fig. 1. Normalized Thermal Neutron and Total Gamma Fluxes Within a Pressurized Water Reactor (PWR) Fuel Cell.

(less than 1%) across the water gap as well as the low sensitivity to changes in the cladding thickness, etc., the use of a power level indicator based on the gamma flux (produced via neutron interactions and the decay of fission products) has the potential for improving the accuracy of the measurement (and thereby reducing the uncertainty). If such a reduction in uncertainty can be translated into a corresponding increase in the operating limits for the same nominal design limits, the impact on electricity production would be significant. A 1% increase in the operating limits would result in approximately four billion additional kilowatt-hours/year from existing nuclear plants. (Plus an additional six billion kW-hr/yr from plants currently planned or under construction.) Furthermore, a reduction of 5-7% in the uncertainty may be possible using the gamma thermometer. Additional advantages of the gamma thermometer are that the GT has the potential for reducing the length of the annual outage for reactors (i.e., through increased reliability and a longer life) and possibly for reducing occupational exposure associated with instrument replacement.

More recently, the possibility of using a slightly modified version of the gamma thermometer as a fluid level indicator has been recognized. A primary concern in the operation of a pressurized water reactor (PWR) is the level of coolant within the reactor vessel. A drop in the coolant level (i.e., uncovering the nuclear core) can result in significant damage to the core, as indicated in the recent Three Mile Island-2 (TMI-2) accident. Due to the extreme environmental conditions present in the core (temperature, pressure, radiation, etc.), no device for the direct measurement of the fluid level is currently available. Past practice has been to infer the coolant level from temperature and pressure measurements of the coolant. This procedure, i.e., indirect measurements and subsequent inferences, can result in ambiguous and possibly incorrect conclusions as to the level of coolant within the core — as in the TMI-2 incident. Since the original gamma thermometer was designed for in-core measurements, it is anticipated that the modified version (i.e., to include fluid level measurement as a second function) would provide a direct, in-core, unambiguous indication of the fluid level and power level within the reactor vessel.

1.1. Technical Summary of the Proposed Gamma Thermometer

1.1.1. Physical Description

The device itself consists of a hollow, cylindrical, stainless steel rod of length equal to (or greater than) the height of the reactor core. At intervals along the rod, annuli of material are removed by machining. A series of differential thermocouples (TCs) are placed at each annulus location, with the TCs and associated electrical leads being in the center of the rod. Once assembled, the cladding (stainless steel, zircalloy, etc.) is swaged onto the exterior in an inert atmosphere (typically Argon). The resulting device is depicted in Fig. 2. The assembled thermometer is then inserted into the center of a fuel assembly (a 17 x 17 array of fuel rods in this study) at the central rod location.

1.1.2. Use of the Gamma Thermometer as a Power Level Monitor

During operation of a nuclear reactor, gamma radiation is produced as a byproduct of the various neutron interaction processes (i.e., fission, capture, etc.) and via decay of fission products. By placing the GT within

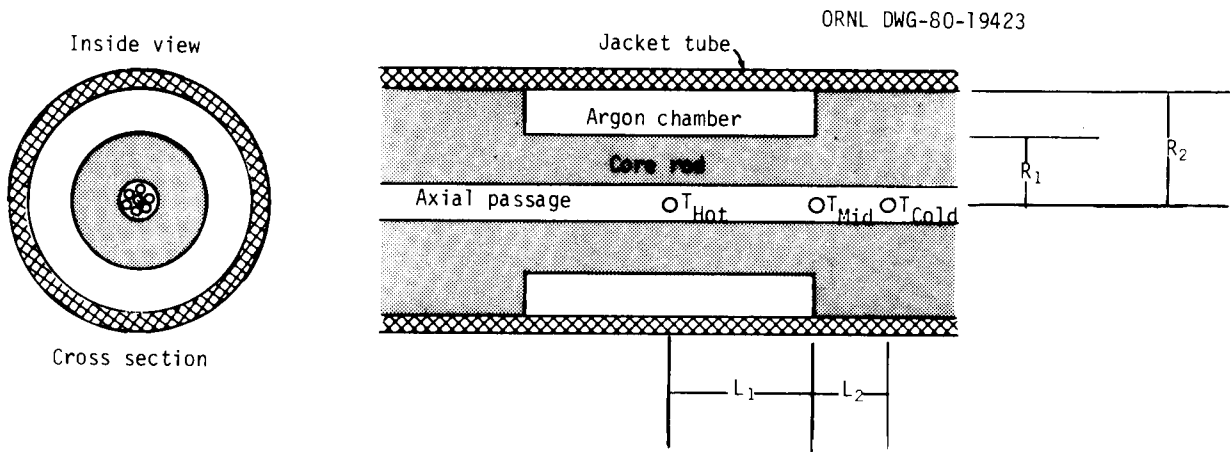


Fig. 2. Schematic of PWR Gamma Thermometer.

a fuel assembly, some fraction of these gamma rays will interact with the stainless steel body of the proposed GT, depositing energy and thus producing heat. The resulting heat will then be transferred from the device to the coolant in which it is immersed. The presence of this volumetric heat source produces a temperature distribution within the device itself. The incorporated thermocouples are used to measure the magnitude of this temperature distribution at two locations (T_{Hot} and T_{Cold} in Fig. 2) within the standard device – with the difference of T_{Hot} and T_{Cold} being used to infer the power level. The relation between the reactor power and the measured temperature difference is roughly approximated as:

$$\Delta T = qL^2/2k \quad (1)$$

where

ΔT = temperature differential between thermocouple junctions, °C

q = heat generation within the thermometer, W/cm³

L = distance between thermocouple junctions in cm

k = thermal conductivity in W/cm °C.

Since q is induced (in part) by the production of gamma rays in fission and fission-product decay (both of which contribute to the linear power of the fuel), Eq. (1) indicates that the temperature difference in the GT can be related to the local heat generation rate.

1.1.3. Use of the Gamma Thermometer as a Fluid Level Indicator

Operation of the gamma thermometer as a fluid level indicator is based on the fact that the heat transfer coefficient on the exterior surface of the device depends on the presence of the reactor coolant and will change dramatically (roughly by a factor of 1,000) when the coolant is removed. The radial heat transfer characteristics at the "hot" and "cold" thermocouple locations are radically different under normal reactor operations (active region of GT immersed in coolant). The radial heat flow at the "hot" thermocouple is sharply reduced due to the gas gap (which functions as an insulator). Therefore the heat flow in this region is principally in the axial direction. By way of contrast, the radial heat flow at the "cold" thermocouple is relatively unrestricted during normal operation. This differential heat transfer results in a higher temperature at the "hot" thermocouple. A loss of coolant on the exterior of the device, however, results in the radial heat transfer properties at both TC junctions becoming similar (i.e., solid/gas interfaces). This will be reflected as a reduced temperature differential between the two thermocouple locations as well as higher absolute temperatures for both locations if the volumetric source remains constant. It is hypothesized that the shape of the temperature distribution (as measured by the thermocouples) can be used to indicate the degree of heat transfer similarity, and hence the presence or absence of the coolant at the level of that particular active region of a "string" of such devices.

1.1.4. Objectives and Scope of Investigation

While the use of the GT in a dual mode is intuitively appealing, it must be noted that the basic arguments advanced in the above discussion are qualitative and not quantitative. Further investigation, both analytical and computational, is clearly required to establish both applications for the gamma thermometer.

This initial investigation, aimed at quantitatively characterizing the GT, included a simplified one-dimensional analytical calculation relating the temperature difference to the various properties (i.e., thermal power, etc.) of the system. Further, a series of two-dimensional transport calculations were executed to relate the volumetric heat source within the GT to the reactor power, together with a series of thermal hydraulic analysis runs utilizing the volumetric heat source to characterize the GT temperature response.

Two objectives were considered in performing the initial analysis. The first objective was directed at establishing the relationship between the gamma thermometer signal and the local power generation rate — a necessary prerequisite to licensing the GT for routine use. The second objective of the computational analysis was to verify the anticipated response of the proposed dual-function gamma thermometer to changes in the fluid characteristics in the nuclear core. The computational effort aimed at realizing these objectives proceeded along two parallel paths: the first dealing with the characterization of the radiation transport from the pin to the detector and the subsequent heat deposition, and the second concerning the thermal hydraulic behavior of the gamma thermometer itself.

It should be noted, however, that the level of analysis required to license the gamma thermometer as either a power level or fluid level indicator is beyond the scope of this report. Rather, the goal of this study was to establish the underlying feasibility of both applications through detailed calculational work so that the pursuit of further efforts for both applications can be justified.

II. THEORETICAL ANALYSIS OF THE DUAL PURPOSE GAMMA THERMOMETER

The use of the gamma thermometer as a dual purpose instrument is dependent on the ability of the device to measure the fluid level within the reactor without compromising its use as a power level monitor. Consequently, the characteristic response used for the power level indicator should be a strong function of the reactor power and a weak function of the heat transfer characteristics and hydraulic environment of the GT. Conversely, the signal utilized for the coolant level indicator must be a weak function of the reactor power and a strong function of the heat transfer and hydraulic characteristics.

A one-dimensional steady state analytical calculation (detailed derivation in the Appendix) was performed on the proposed gamma thermometer design (see Fig. 2) to characterize the thermocouple signals. The results of the analysis, shown below in Eqs. (2) and (3), depict the temperatures at both TC locations as functions of power and heat transfer characteristics,

$$(T_{\text{Hot}} - T_{\text{Coolant}}) = \frac{qL_1^2}{2k} + \frac{\frac{qL_1R_1^2}{kmR_2^2} (1 + e^{-2mL_2})}{(1 - e^{-2mL_2})} + \frac{q}{m^2k} \quad (2)$$

$$(T_{\text{Cold}} - T_{\text{Coolant}}) = \frac{\frac{2qL_1R_1^2}{kmR_2^2} e^{-mL_2}}{(1 - e^{-2mL_2})} + \frac{q}{m^2k} \quad (3)$$

where $m^2 = \frac{hP}{kA}$ and the remaining terms are defined in Fig. 2 or in the Appendix. As stated above, the difference between the two TC readings is utilized to infer the local heat generation rate. Subtracting Eq. (3) from Eq. (2) yields:

$$(T_{\text{Hot}} - T_{\text{Cold}}) = \frac{qL_1^2}{2k} + \frac{\frac{qL_1R_1^2}{kmR_2^2} \left[\frac{(1 + e^{-2mL_2}) - 2e^{-mL_2}}{(1 - e^{-2mL_2})} \right]}{\quad} \quad (4)$$

which as desired, is a strong function of the local power (via q) and a weak function of the heat transfer properties (via m). The functional dependence of the GT signal on local power is depicted graphically in Fig. 3.

In light of the desire to produce a fluid level response with the opposite characteristics, a simple expedient is to divide Eq. (2) by Eq. (3) (thereby eliminating the dependence on q), giving:

$$\frac{(T_{\text{Hot}} - T_{\text{Coolant}})}{(T_{\text{Cold}} - T_{\text{Coolant}})} = \frac{\frac{L_1^2}{2} (1 - e^{-2mL_2}) + \frac{L_1 R_1^2}{m R_2^2} (1 + e^{-2mL_2}) + \frac{1}{m^2} (1 - e^{-2mL_2})}{\frac{2L_1 R_1^2}{m R_2^2} e^{-mL_2} + \frac{1}{m^2} (1 - e^{-2mL_2})} \quad (5)$$

Figure 4 illustrates the relationship shown in Eq. (5), and verifies the strong dependence of the ratio of the thermocouple signals on the exterior heat transfer coefficient. Although Eq. (5) possesses the desired characteristics, the ratio specified requires that additional information be incorporated into the response. In particular, it requires that two absolute temperature measurements (or one absolute and one differential measurement) be available as well as an external measurement of the coolant temperature.

An alternative response that is also insensitive to the power level can be constructed by utilizing an additional temperature measurement at a point between the "hot" and "cold" junctions given as T_{Mid} in Fig. 2. Similar to the relationship given in Eqs. (1) and (2), the temperature at this point is given by;

$$(T_{\text{Mid}} - T_{\text{Coolant}}) = \frac{\frac{q L_1 R_1^2}{k m R_2^2} (1 + e^{-2mL_2})}{(1 - e^{-2mL_2})} + \frac{q}{m^2 k} \quad (6)$$

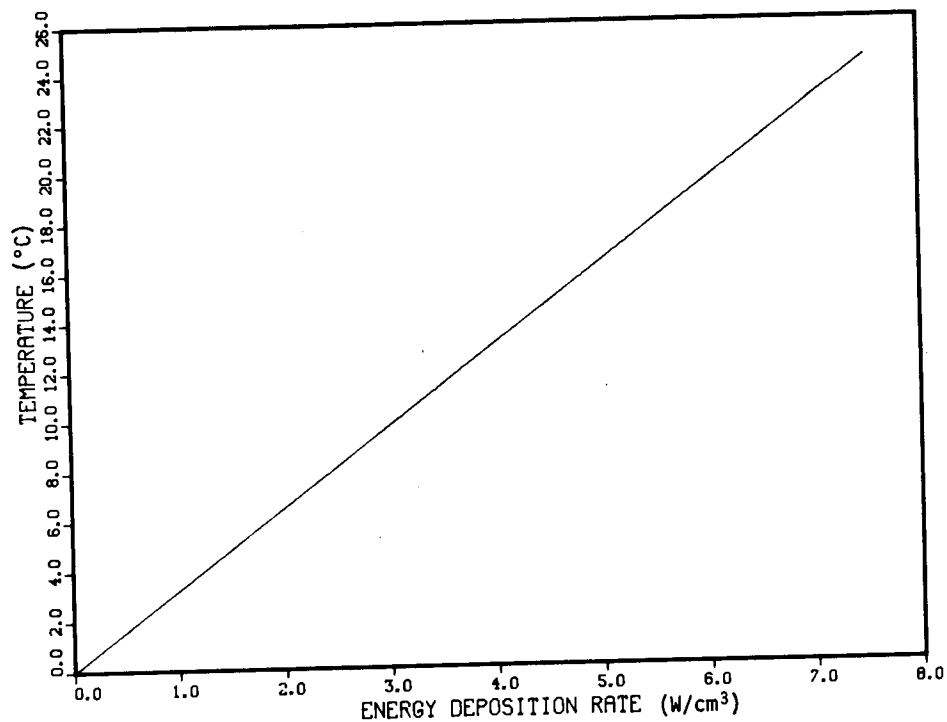


Fig. 3. Theoretical Power Level Response Characteristics of the Gamma Thermometer.

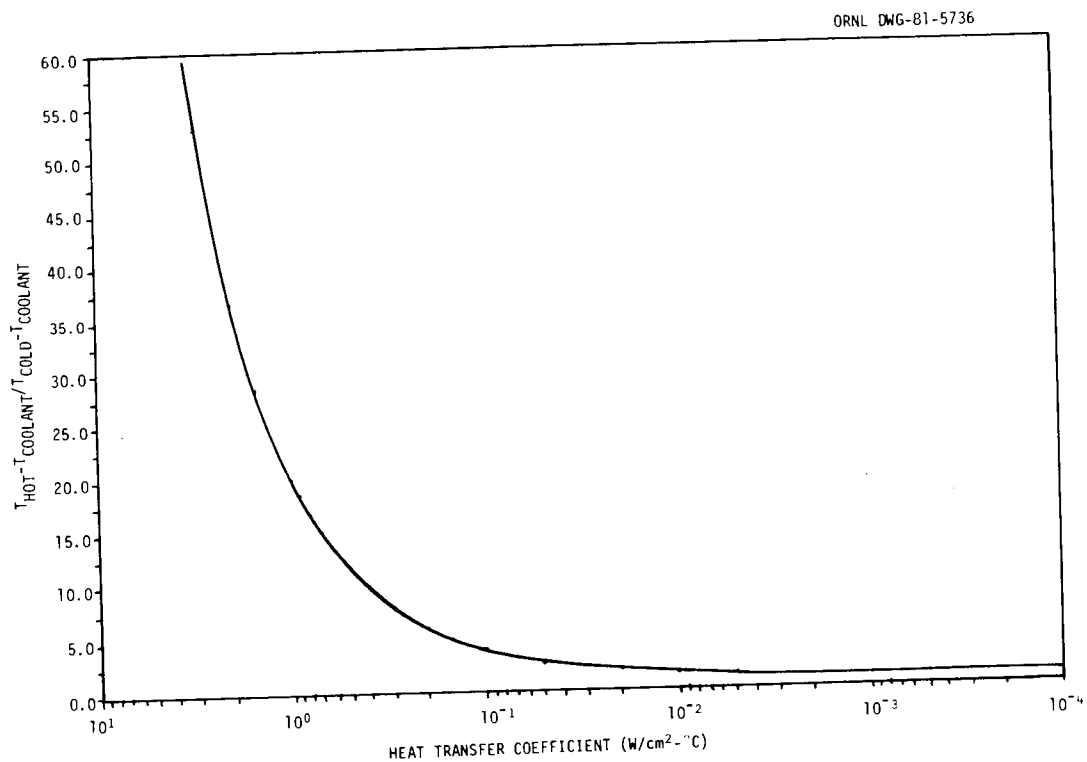


Fig. 4. Theoretical Fluid Level Response Characteristics of GT Using Coolant Temperature as Reference Temperature.

so that the proposed fluid level response is given by:

$$\frac{(T_{\text{Hot}} - T_{\text{Mid}})}{(T_{\text{Mid}} - T_{\text{Cold}})} = \frac{\frac{mL_1 R_2^2}{2R_1^2} (1 - e^{-2mL_2})}{\left[(1 + e^{-2mL_2}) - 2e^{-mL_2} \right]} \quad (7)$$

A plot of the fluid level response as indicated by Eq. (7) is shown in Fig. 5, indicating the strong dependence on the surface heat transfer coefficient.

Analogous to Eq. (5), this response is nominally independent of power level. Moreover, it requires no information not available from thermocouple measurements within the gamma thermometer (i.e., the instrument is self-contained). A relatively straightforward manner of obtaining the requisite information is to incorporate two differential thermocouples per active location; the first measuring $T_{\text{Hot}} - T_{\text{Mid}}$, the second measuring $T_{\text{Mid}} - T_{\text{Cold}}$. The required power level signal could then be constructed by summing the two differential thermocouple signals.

Equations (4) and (7) indicate that the gamma thermometer can theoretically function as a dual purpose monitoring device. The use of Eq. (4) as a response provides an indication of the local heat generation rate in the reactor region in the vicinity of the GT. Using Eq. (7) as a response, the local thermal hydraulic conditions can be monitored. Hence using "strings" of active locations spaced radially within the reactor core, both a power map and a coolant level indication can be obtained via the GT.

Although the above theoretical analysis illustrates the feasibility of utilizing the GT as a dual purpose measuring device, many of the simplifying assumptions which were used in the analysis must be evaluated as to their effect on the results. Due to the coupled non-linear inhomogeneous nature of the GT heat conduction problem, the multi-dimensional analysis was treated via numerical techniques. In particular, radiation transport

analysis was used to characterize the volumetric heat generation rate as a function of reactor power, and thermal hydraulic analysis was used to relate the exterior heat transfer coefficient to changes in the fluid level.

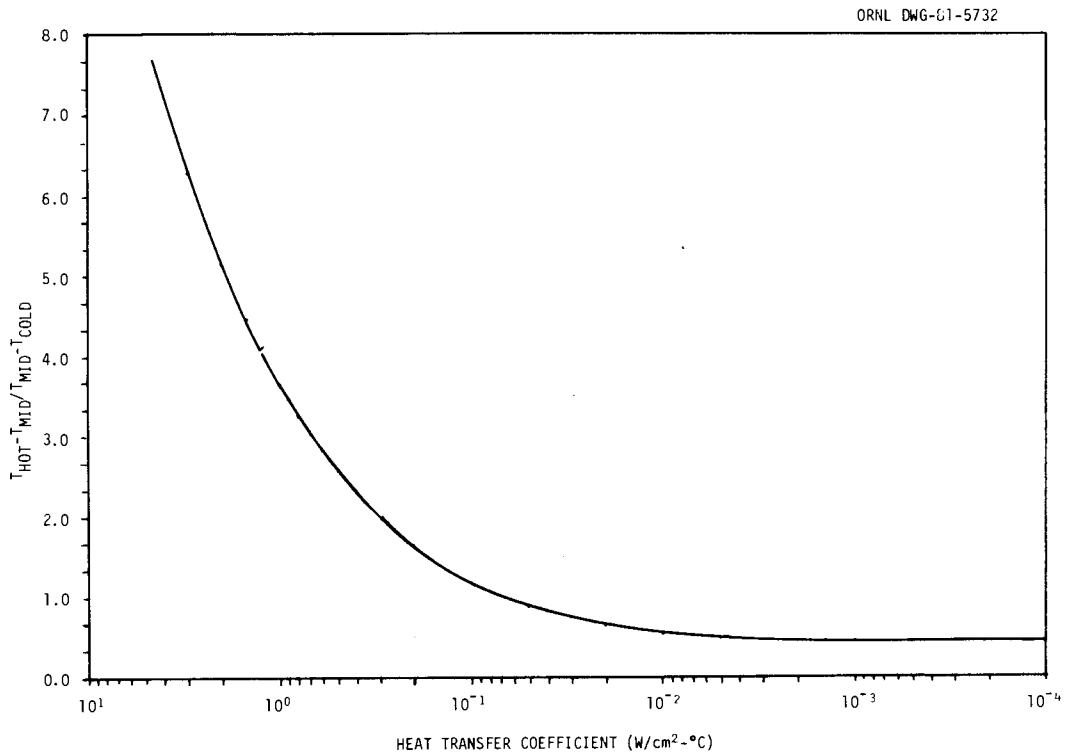


Fig. 5. Theoretical Fluid Level Response Characteristics of GT Using Internal Reference Temperature.

III. RADIATION TRANSPORT ANALYSIS

As noted previously, a primary objective of this study is to relate the energy deposition within the GT (i.e., q in Eqs. 1-7) to the local heat generation rate occurring within the fuel pins. Such a characterization must include the source of the particles involved (i.e., geometrically within the reactor), the origin of the particles (i.e., neutron-induced reactions or fission product decay), and also the manner in which the particles (which can be viewed as containing information regarding the state of the reactor) actually reach the detector. The results of just such a characterization are reported in this section.

A prototypic PWR fuel assembly consisting of 288 pins in a square lattice (17×17) was selected as the basis for this investigation. The design parameters for this assembly are given in Table 1. The central pin of the 17×17 array was replaced by the gamma thermometer, and all other pins contained UO_2 fuel (i.e., control rods were not modeled to simplify the calculations.) The axial mid-plane of the assembly was modeled in two-dimensional x-y geometry as indicated in Fig. 6. Due to the assumed symmetry conditions, only one-fourth of the assembly was actually calculated. The materials and number densities comprising the various regions are given in Table 2. In the numerical transport analysis, a 5×5 array of nodes was used within the gamma thermometer itself for the purpose of obtaining the spatial distribution of the energy deposition.

Due to the difference in the transport processes of neutrons and gamma radiation in a moderating medium, standard reactor core analysis methods (i.e., diffusion theory) are inadequate to accurately model the transport of gamma rays. However, the methods typically employed in radiation shielding applications (e.g. particle transport theory) are appropriate calculational tools.

Nuclear parameters for the various materials were taken from the 27 neutron energy group, 18 gamma energy group coupled cross-section library.⁴ This library has been extensively utilized for LWR shielding calculations. The AMPX-II³ modular cross-section processing system was utilized to reduce the 27n-18 γ group library (which contains 12 thermal

Table 1. Design Parameters Used in the Radiation Transport and Thermal Hydraulic Calculations

Rated heat output (core), Mw(Th)	3,760
System pressure (nominal), Pa	1.5513×10^7
Average coolant flow velocity, cm/s	513.59
Average coolant temperature, °C	300
Fuel rod pitch, cm	1.2776
Overall dimension of fuel assembly (side of square), cm	21.9253
Number of fuel rods per assembly	288*
Outside diameter of fuel rod, cm	0.96266
Diametral gap, cm	0.02032
Cladding thickness, cm (Zircalloy 2)	0.05969
Active fuel length, cm	363.22
Fuel pellet (UO ₂ sintered) density, % of theoretical	94.0
Fuel pellet diameter, cm	0.82296
Average fuel discharge burnup, Mwd/tonne U	33,700
Average fuel enrichment, wt% ²³⁵ U	3.18
Effective multiplication (beginning of life)	1.333

*Assumes no control rods, and one fuel rod replaced with the gamma thermometer.

neutron groups with upscatter) to a 15n-18 γ group library with one thermal group (and hence no upscatter). The NITAWL³ and XSDRNPM³ modules were utilized to perform the requisite resonance self-shielding and cell weighting (single pin) calculations respectively.

In order to calculate the energy deposition rate within the stainless steel core of the gamma thermometer, two sources of gamma radiation must be considered: the gammas resulting from neutron-induced reactions (fission, capture, and inelastic scattering) and the gammas produced by the decay of the various fission products. The response function utilized for both sources of gamma radiation was the energy deposition rate for stainless steel given in Table 3. The energy deposition rate due to the

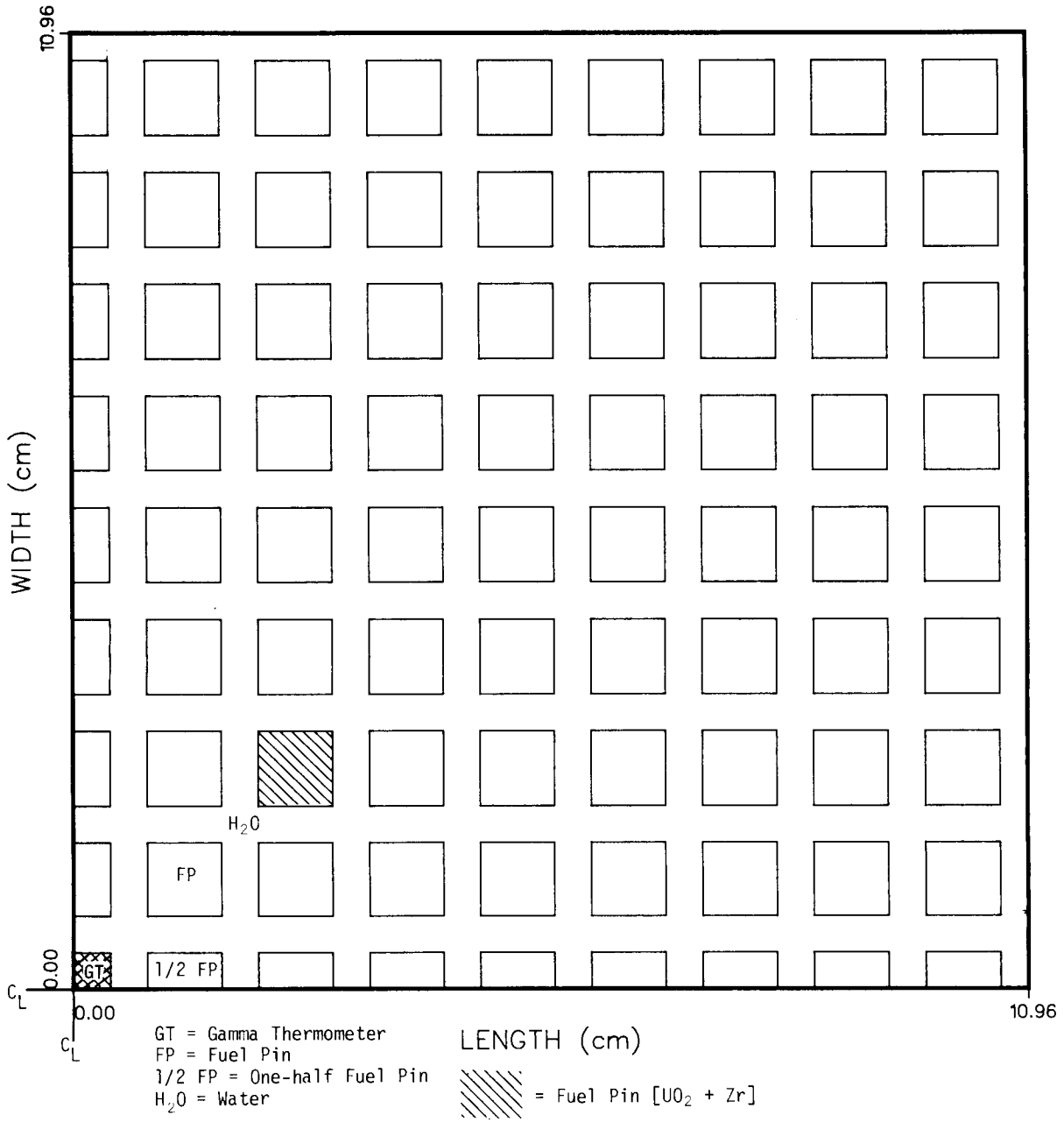


Fig. 6. Calculational Model of the Prototypic PWR Fuel Assembly Used for Radiation Transport Calculations.

Table 2. Materials and Number Densities Used in Radiation Transport Calculation

Mixture	Material	Number Density (atoms/cm ³)
Water	H	6.692+22
	O	3.346+22
	B ¹⁰	1.0+4*
	B ¹¹	1.0+4*
UO ₂	U ²³⁵	7.4503+20
	U ²³⁸	2.2684+22
	Pu ²³⁹	1.0+4*
	Pu ²⁴⁰	1.0+4*
	O	4.68573+22
Zircalloy	Zr-2	4.2945+22
SS-3162	C	3.1454+20
	Si	1.6828+21
	P	6.8612+19
	S	4.4186+19
	Cr	1.5434+22
	Mn	1.7193+21
	Fe	5.5248+22
	Ni	9.6549+21
Mo	1.2303+21	

*Included for sensitivity studies.

neutron induced reactions was computed via an eigenvalue calculation using the coupled neutron-gamma library and normalized to a fission rate corresponding to 186 W/cm. The DOT-IV⁵ computer code was utilized for all radiation transport calculations. In most cases, a P₃ scattering approximation and an S₈ quadrature set (48 directions) were employed.

The fission product decay contribution was calculated using only the gamma groups and assuming a uniform fixed source in each fuel pin. The

Table 3. Input Source and Response Functions
for the Radiation Transport Calculations

Energy Group	Top Boundaries (MeV)	Energy Deposition function for SS-316 $\frac{\text{W/cm}^3}{\text{photons/cm}^2 \cdot \text{s}}$	Decay Spectrum (photons/source photon)	Fission Gamma Spectrum (photons/source photon)
1	10.0	2.60332-13	3.1664-08	1.51-04
2	8.0	1.98855-13	5.6180-07	7.56-04
3	6.5	1.53348-13	2.1160-04	3.18-03
4	5.0	1.18533-13	1.1987-03	8.19-03
5	4.0	9.21595-14	2.6834-03	2.46-02
6	3.0	7.36853-14	5.1678-03	2.70-02
7	2.5	6.21629-14	1.1508-02	4.69-02
8	2.0	5.27663-14	1.1854-02	5.52-02
9	1.66	4.51833-14	3.0783-02	7.11-02
10	1.33	3.73517-14	4.4051-02	9.59-02
11	1.0	3.04364-14	6.6178-02	8.67-02
12	0.8	2.47022-14	9.7403-02	1.02-01
13	0.6	1.86513-14	8.1859-02	1.25-01
14	0.4	1.43561-14	5.3713-02	7.27-02
15	0.3	1.27314-14	8.5042-02	8.60-02
16	0.2	1.77316-14	1.2598-01	9.09-02
17	0.1	5.60685-14	1.3196-01	5.07-02
18	0.05	4.84837-13	2.5044-01	4.26-02
	0.01			

gamma energy spectrum and source strength for the fission product contribution were determined using ORIGEN⁶ at a burnup of approximately 33,800 MWD/MTHM. The gamma source spectrum utilized is also given in Table 3.

A third transport calculation was performed (again utilizing only the gamma groups) to estimate the contribution due solely to prompt gammas from the fission reaction. This calculation assumed a uniform fixed

source in each fuel pin with the distribution of source gammas per fission shown in the last column of Table 3.

The actual location of the fuel assembly containing the gamma thermometer in the core grid pattern may have a direct effect on the energy deposition rate within the gamma thermometer, due to the non-uniform flux distribution in the radial direction of the reactor core. To assess this effect (i.e., the uncertainty in the location of the instrumented fuel assemblies), the preliminary investigation included two cases which utilized boundary conditions for the radiation transport calculations representing extreme conditions. A case study was performed on the two fixed source calculations (fission source and fission product decay source) utilizing fully reflected boundary conditions (i.e., infinite lattice of fuel assemblies) on all sides. A second case study was performed for the same two fixed source calculations utilizing vacuum boundary conditions (an isolated element) on all sides. The results of this analysis (see Table 4) show approximately 94% of the fission gammas (and 96% of the fission product gammas) originate within the instrumented fuel element. This result indicates that the response of the gamma thermometer will be relatively insensitive to the actual location of the instrumented fuel assembly within the reactor core. Therefore, the remainder of this report (unless otherwise stated) will consider the fully reflected case only.

Table 4. Fraction of Total Response Due to Gammas Originating within the Fuel Element Containing the Gamma Thermometer

Source	Percentage of Signal
Fission	0.9382
Decay	0.9597

One overall objective of the forward transport analysis was to determine the spatial distribution of the energy deposition within the gamma thermometer. The results of that analysis are shown in Figs. 7-10. Figures 7 and 8 represent the fixed source calculations using the fission source gamma distribution and decay source gamma distribution respectively. Figure 9 represents the coupled 15n-18 γ group eigenvalue calculation for the energy deposition due to all neutron induced reaction. The results of all three figures indicate a relatively flat spatial distribution within the gamma thermometer with the maximum spatial deviation from the center-line value being approximately 6%. A second significant result of the calculation can be discerned by comparing Figs. 7 and 9. This result exemplifies the importance of the other (non-fission) neutron induced reactions to the total heat deposition rate.

Approximately 49% of the total neutron induced response is due to the fission reaction alone. An interesting sidelight to this result was the different spatial distributions of the response due to fission gammas and the response due to all other neutron-produced gammas. The spatial distribution shift is believed to be a function of both the energy distribution of the source gammas coupled with the energy dependence of the response function. A detailed characterization of this effect, however, was not pursued. The total source in Fig. 10 is the sum of Fig. 8 and 9, and represents the total gamma energy deposited in the gamma thermometer during normal operation of a PWR. [It should be noted that this analysis does not account for the direct neutron heating of the gamma thermometer.]

The fractional breakdown of the total source in Fig. 10 by gamma production process (i.e., fission-product decay, fission, other) is depicted in Figs. 11-13. These results indicate a total response breakdown of approximately 22.0% fission product decay gammas, 37.3% fission gammas, and 40.7% other neutron-induced gammas (i.e., capture, inelastic).

As a secondary objective, the spatial distribution of the source gammas contributing to the effect of interest was also characterized. To this end, a set of adjoint gamma transport calculations was executed.

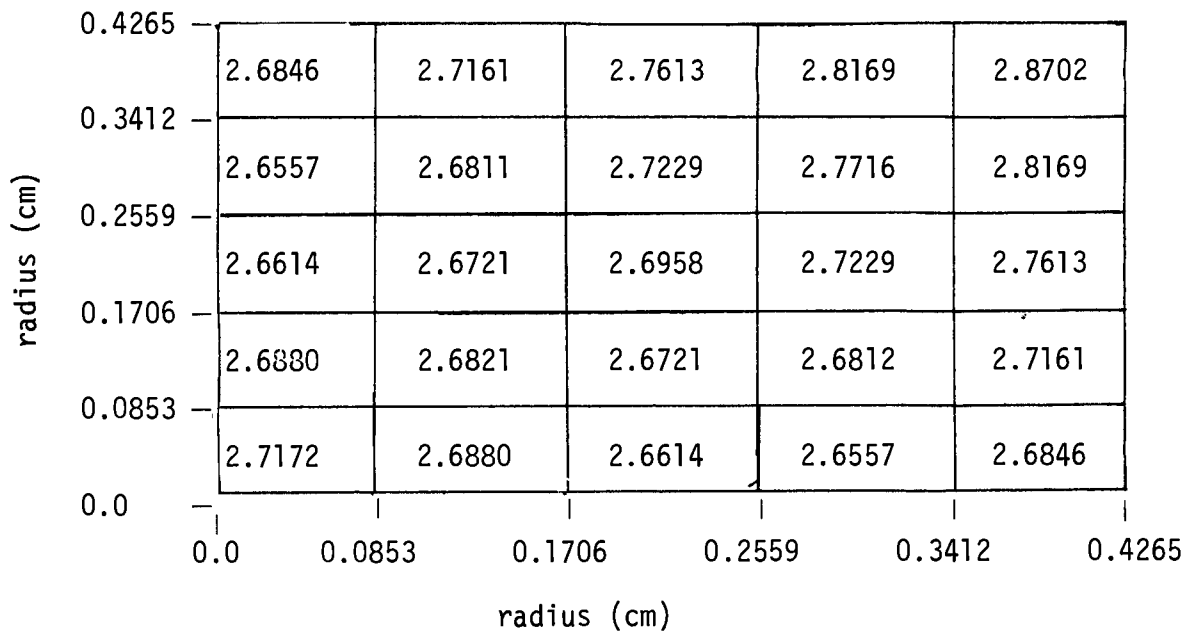


Fig. 7. Volumetric Energy Deposition Rate Distribution in the Gamma Thermometer Due to Fission Source (W/cm^3).

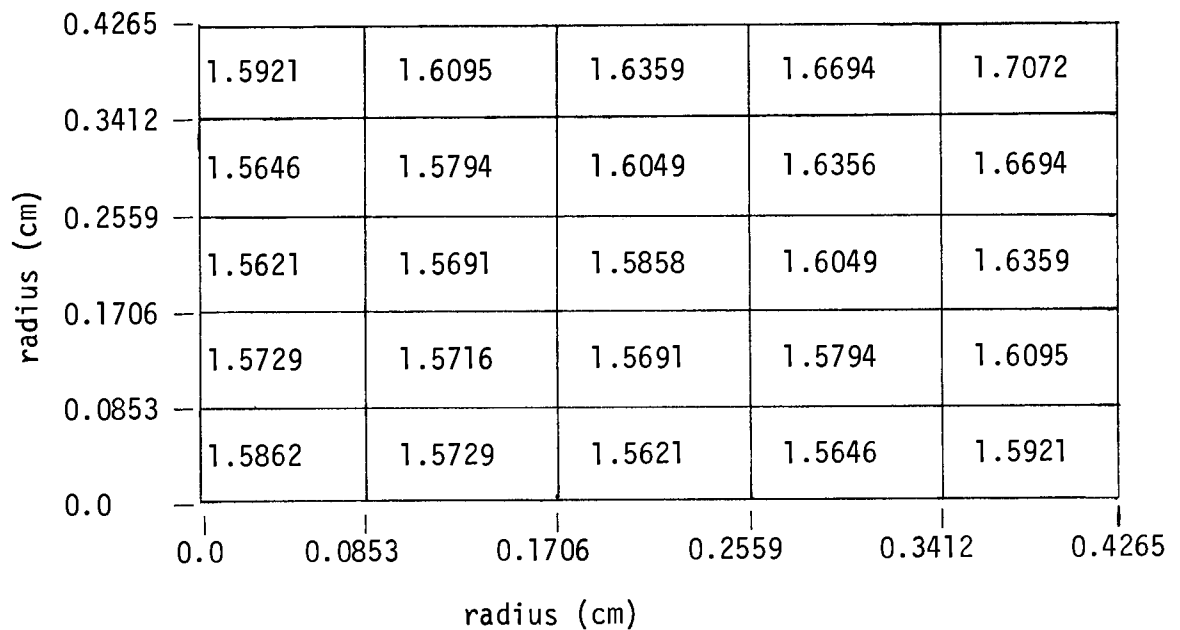


Fig. 8. Volumetric Energy Deposition Rate Distribution in the Gamma Thermometer Due to Fission Product Decay Source (W/cm^3).

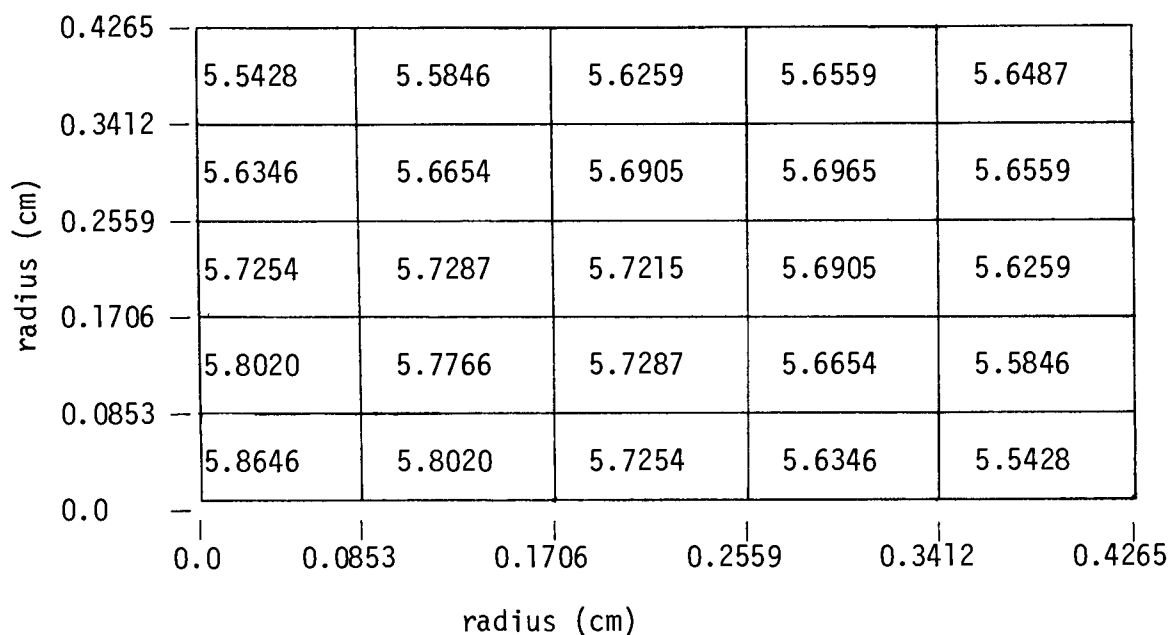


Fig. 9. Volumetric Energy Deposition Rate Distribution in the Gamma Thermometer Due to All Neutron Induced Reactions (W/cm^3).

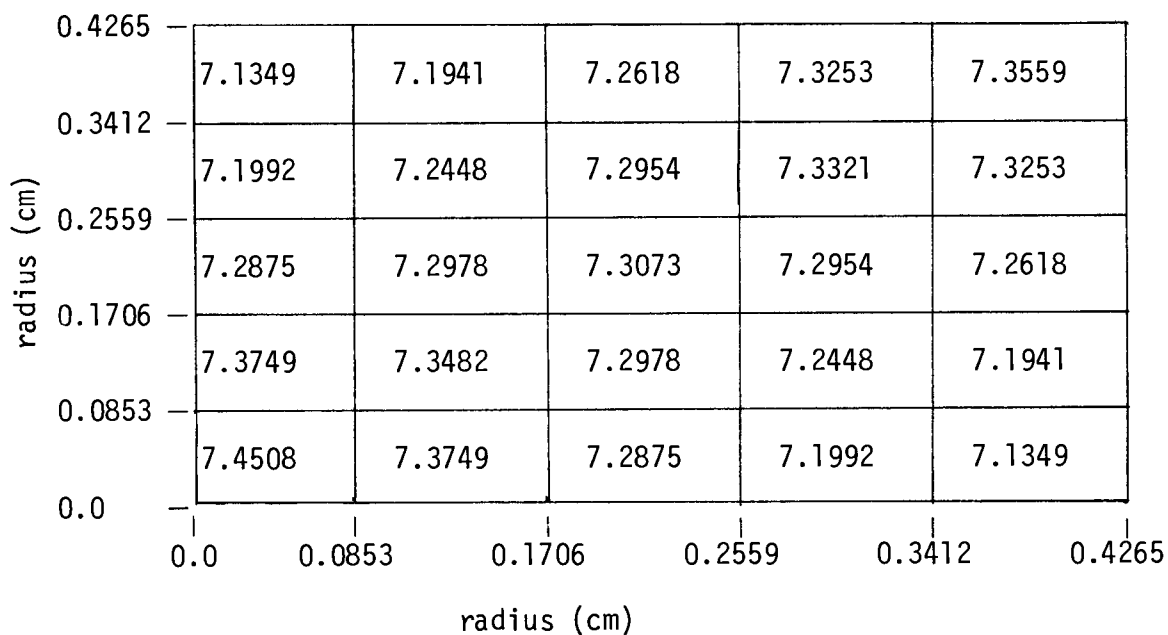


Fig. 10. Total Volumetric Energy Deposition Rate Distribution in the Gamma Thermometer Due to All Sources (Decay + Neutron Induced) [W/cm^3].

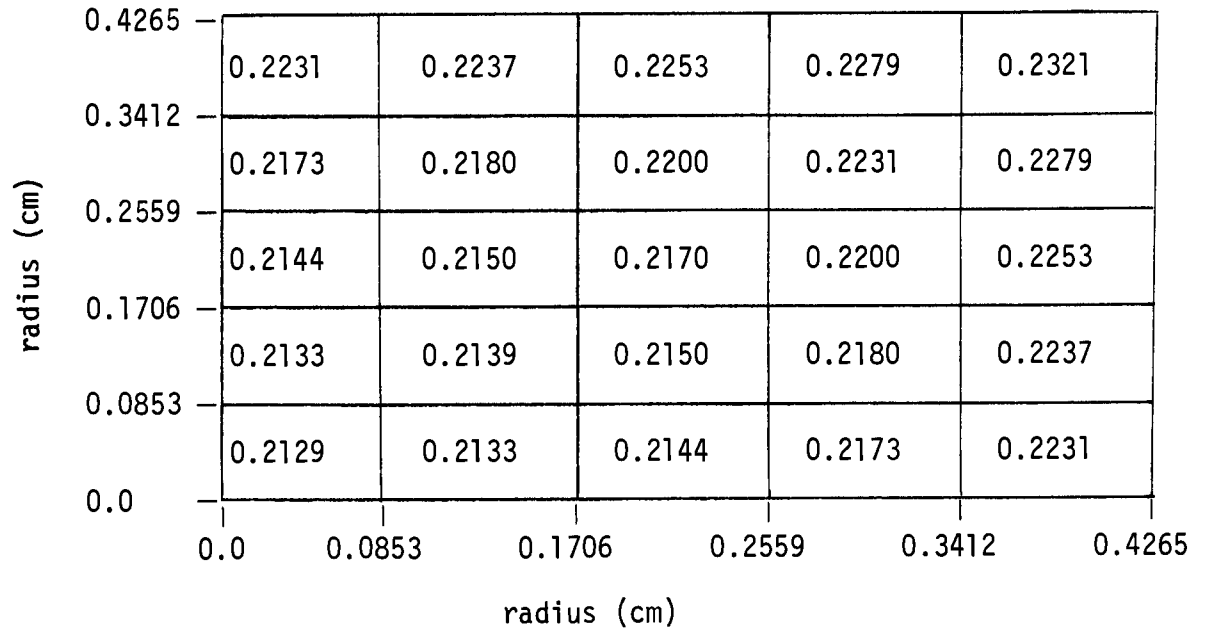


Fig. 11. Fraction of Total Volumetric Energy Deposition Rate Distribution in the Gamma Thermometer Due to Fission Product Decay Gammas.

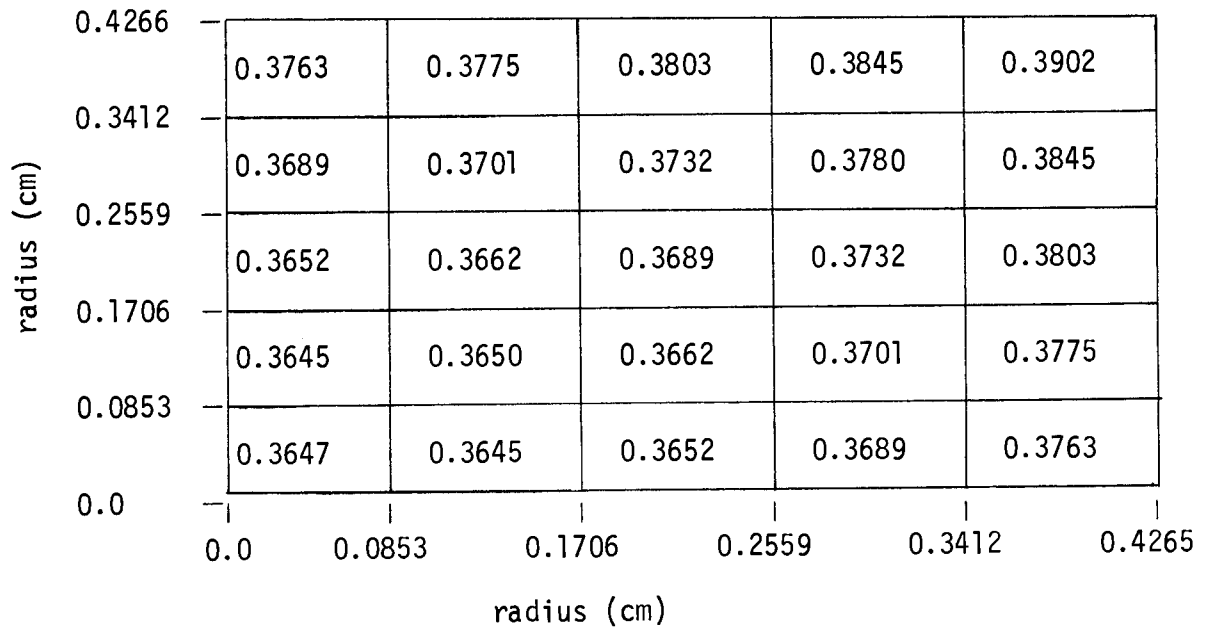


Fig. 12. Fraction of Total Volumetric Energy Deposition Rate Distribution in the Gamma Thermometer Due to Fission Gammas.

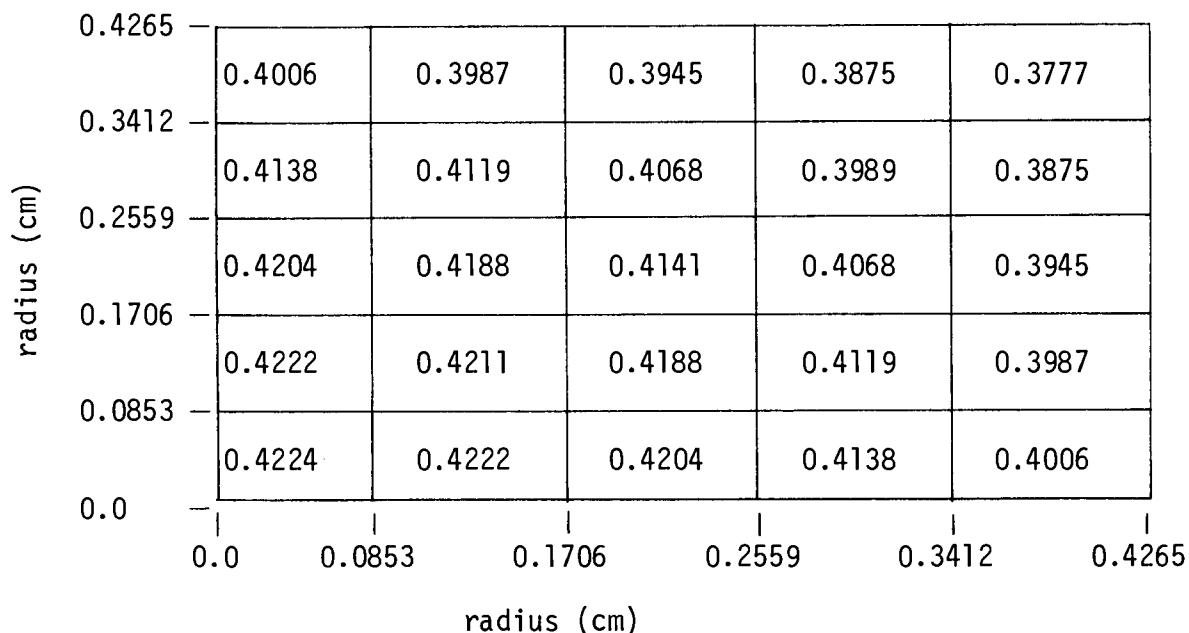


Fig. 13. Fraction of Total Volumetric Energy Deposition Rate Distribution in the Gamma Thermometer due to All Neutron Induced Reactions Other Than Fission.

The logical $15n-18\gamma$ group coupled adjoint case, was not executed because the DOT-IV code does not yet include provisions for such a generalized adjoint calculation (i.e., fixed source in a critical reactor.) The source for the adjoint cases was the response function (see Table 3) used in the forward transport analysis (i.e., the energy deposition function for stainless steel). The response functions for the adjoint transport analysis were the fission gamma source spectrum and fission product decay gamma source spectrum also presented in Table 3.

Analysis of the initial adjoint calculations (S_8-48 directions) indicated that the phenomenon known as "ray effects" was present in the calculations. Due to the localized source within the low scattering medium, the discrete ordinates approximation biased the particle flow in certain directions (i.e., the 48 discrete angles). To mitigate these "ray effects," an adjoint transport calculation was executed utilizing 664 directions and no scattering. A first collision source was then formed for use in a second adjoint transport calculation utilizing the original S_8 quadrature. This procedure effectively eliminated the problem

of the "ray effects," and the results of this latter calculation were employed to determine the fractional contribution to the energy deposition rate due to source gammas originating in each fuel pin.

The radial characterization of the gamma source is presented in Tables 5 and 6. Only the prompt fission gamma and fission product decay gamma data were calculated. In both tables, each box represents a fuel pin. In comparing Tables 5 and 6, the results showed that the fractional contribution due to decay gammas is higher in the rows immediately adjacent to the gamma thermometer and lower in the fuel pin rows farther away when compared to the contributions due to prompt fission gammas. This result is seen more clearly in Table 7 which shows approximately 68% of the fission induced gammas originating in the first three rows of elements whereas approximately 75% of the fission product decay gammas originate in the first three rows for the fully reflected case. Likewise, the results show a 72%-78% split for the void case. These results indicate that the gamma thermometer is, as desired, strongly dependent on the localized power generation rate.

To further characterize the forward gamma source, and to investigate the contributions of the various gamma-producing neutron interactions, a sensitivity study was performed. Using the coupled $15n-18\gamma$ group eigenvalue fluxes and the adjoint 18γ group fluxes, the contribution flux ($\phi\phi^*$) by material region was calculated using the VIP⁷ computer code. The sensitivity analysis was performed using SWANLAKE⁸ to fold the contribution flux with a partial cross section sensitivity library (i.e., the $15n-18\gamma$ group library broken up by reaction). The results of the sensitivity analysis by mixture and significant neutron reaction are presented in Table 8 with the results by element and neutron reaction for the materials presented in Tables 9-11.

The primary gamma producing neutron reactions were found to be the (n,γ) , (n,f) , and $(n,n'\gamma)$ reactions. The results in Table 8 show that the (n,γ) and (n,f) reactions predominate with approximately the same percentage split (bottom row total) shown in Figs. 12 and 13 of the volumetric energy deposition rate data. The discrepancy between the two results is contained within the miscellaneous column of Table 8. This column represents the percentage of the response originating from certain high energy

Table 5. Fractional Contribution by Fuel Pin to the Total Volumetric Energy Deposition Rate in the GT Due to Fission for Reflected (Void) Boundary Conditions

Row 9	0.00044 (0.00025)	0.00080 (0.00047)	0.00118 (0.00068)	0.00078 (0.00041)	0.00062 (0.00033)	0.00056 (0.00027)	0.00056 (0.00027)	0.00056 (0.00022)	0.00050 (0.00017)
8	0.00053 (0.00039)	0.00102 (0.00080)	0.00128 (0.00096)	0.00090 (0.00060)	0.00071 (0.00047)	0.00066 (0.00043)	0.00063 (0.00039)	0.00056 (0.00029)	
7	0.00074 (0.00063)	0.00158 (0.00141)	0.00152 (0.00129)	0.00115 (0.00088)	0.00094 (0.00074)	0.00091 (0.00072)	0.00071 (0.00050)		
6	0.00114 (0.00104)	0.00266 (0.00252)	0.00199 (0.00182)	0.00159 (0.00137)	0.00150 (0.00132)	0.00108 (0.00091)			
5	0.00198 (0.00187)	0.00447 (0.00434)	0.00300 (0.00284)	0.00272 (0.00253)	0.00197 (0.00179)				
4	0.00414 (0.00406)	0.00746 (0.00735)	0.00540 (0.00526)	0.00416 (0.00399)					
3	0.01166 (0.01157)	0.01460 (0.01452)	0.01034 (0.01024)						
2	0.04950 (0.04944)	0.03709 (0.03701)							
1	Gamma Thermometer								
Column	1	2	3	4	5	6	7	8	9

Table 6. Fractional Contribution by Fuel Pin to the Total Volumetric Energy Deposition Rate in the GT Due to Fission Product Decay for Reflected (Void) Boundary Conditions

Row 9	0.00032 (0.00018)	0.00059 (0.00035)	0.00086 (0.00041)	0.00056 (0.00030)	0.00042 (0.00022)	0.00038 (0.00019)	0.00038 (0.00018)	0.00037 (0.00015)	0.00033 (0.00012)
8	0.00040 (0.00031)	0.00077 (0.00061)	0.00097 (0.00074)	0.00065 (0.00045)	0.00050 (0.00035)	0.00046 (0.00032)	0.00043 (0.00027)	0.00038 (0.00020)	
7	0.00059 (0.00052)	0.00125 (0.00114)	0.00120 (0.00105)	0.00086 (0.00068)	0.00069 (0.00057)	0.00067 (0.00054)	0.00050 (0.00037)		
6	0.00096 (0.00089)	0.00223 (0.00214)	0.00163 (0.00153)	0.00125 (0.00111)	0.00117 (0.00106)	0.00081 (0.00069)			
5	0.00173 (0.00167)	0.00404 (0.00396)	0.00260 (0.00250)	0.00229 (0.00217)	0.00157 (0.00146)				
4	0.00382 (0.00377)	0.00732 (0.00726)	0.00501 (0.00493)	0.00358 (0.00348)					
3	0.01172 (0.01168)	0.01558 (0.01551)	0.01002 (0.00995)						
2	0.05972 (0.05960)	0.04334 (0.04328)							
1	Gamma Thermometer								
Column	1	2	3	4	5	6	7	8	9

Table 7. Fractional Contribution by Fuel Pin Row to the Total Volumetric Energy Deposition Rate

Row	Number of Fuel Pins	Fission (Ref1)	Decay (Ref1)	Fission (Void)	Decay (Void)
1	0				
2	8	0.3462	0.4121	0.3686	0.4291
3	16	0.2047	0.2115	0.2168	0.2196
4	24	0.1360	0.1282	0.1418	0.1319
5	32	0.0972	0.0847	0.0984	0.0850
6	40	0.0707	0.0575	0.0682	0.0554
7	48	0.0545	0.0417	0.0478	0.0368
8	56	0.0461	0.0334	0.0340	0.0250
9	64	0.0446	0.0809	0.0244	0.0172

neutrons. Above a certain energy, which is material dependent, the cross-section evaluations do not distinguish which neutron reaction produces the gamma ray.⁹ Therefore a separate cross section was formulated to account for these gammas.

An alternate characterization of the neutron-induced response yields 2% originating in the water, 83% originating in the fuel, and 15% originating within the thermometer itself. The 2% of the response originating in the water is due entirely to the (n,γ) reaction in Hydrogen as seen in Table 9. It should be noted that the $(n,n'\gamma)$ reaction had no contribution in the water. In Table 10, the results for the UO_2 fuel pins are presented. Considering the last column in Table 10, the results show 67% of the UO_2 contribution originating from U^{235} , and 33% from U^{238} . An interesting result seen in the U^{238} row is that most of the (Misc) signal for the UO_2 mixture (and also for the total - Table 8) originates from the high energy neutron interaction with U^{238} . The Zr-2 mixture was found to have no gamma production cross section and therefore had no contribution to the response. The stainless steel (SS-316L) results (by element) presented in Table 11 show the (n,γ) reaction as the dominant neutron reaction for production of contributory gammas within the thermometer itself.

Table 8. Fractional Contribution by Mixture and Reaction of the Neutron Induced Gammas to the Volumetric Energy Deposition Rate

Reaction	(n, γ)	(n,f)	(n,n' γ)	(Misc)	Total
Material					
H ₂ O	1.91284-02	0.0	3.44843-22	0.0	1.91284-02
UO ₂ -Zr2	3.17582-01	4.40844-01	2.28209-05	6.89472-02	8.27396-01
SS-316L	1.34426-01	0.0	2.38859-03	1.66635-02	1.53478-01
Total	4.71136-01	4.40844-01	2.41141-03	8.56107-02	1.0000

Table 9. Fractional Contribution by Material and by Reaction to the Total Volumetric Energy Deposition Rate Due to Water

Reaction	(n, γ)
Material	
H	1.91194-02
O	9.09198-06
Total	1.91284-02

Table 10. Fractional Contribution by Material and by Reaction of the Total Volumetric Energy Deposition Rate Due to UO₂

Reaction	(n, γ)	(n,f)	(n,n' γ)	(Misc)	Total
Material					
0	6.61536-06	0.0	0.0	0.0	6.61536-06
U ²³⁵	1.12509-01	4.40839-01	2.28209-05	3.34864-03	5.56719-01
U ²³⁸	2.05066-01	4.45528-06	0.0	6.55986-02	2.70669-01
Total	3.17582-01	4.40844-01	2.28209-05	6.89472-02	8.27396-01

Table 11. Fractional Contribution by Material and by Reaction of the Total Volumetric Energy Deposition Rate Due to Stainless Steel (SS-316L)

Reaction	(n, γ)	(n,n' γ)	(Misc)	Total
Material				
Cr	2.67908-02	0.0	3.82903-03	3.06198-02
Mn	1.15247-02	0.0	2.94098-04	1.18188-02
Fe	6.47059-02	2.27099-03	9.87389-03	7.68508-02
Ni	2.48352-02	0.0	1.93359-03	2.67688-02
Mo	6.41044-03	0.0	7.25604-04	7.13604-03
Trace Elements C,Si,S,P	1.58832-04	1.17595-04	7.3794-06	2.8381-04
Total	1.34426-01	2.38859-03	1.66635-02	1.53478-01

Another aspect of Tables 9-11 is shown in Tables 12-14 which presents the sensitivity coefficients for the various materials and reactions responsible for the gamma heating source. Therefore, a change in the response (i.e., the energy deposited in the GT) can be estimated for changes in the various mixtures utilized in the reactor core as shown

$$\Delta R = \sum_{\substack{\text{materials} \\ \text{reactions}}} \langle \phi_{\gamma}^* \sigma_{\gamma \leftarrow n}, \phi_n \rangle \Delta N_i \quad (8)$$

where ΔN_i is a change in a material number density (in units of atoms/b-cm) and the bracket is used to indicate a volume integration over the assembly. The term in the bracket (i.e., $\langle \phi_{\gamma}^* \sigma_{\gamma \leftarrow n}, \phi_n \rangle$) thus represents the gamma-production sensitivity coefficients and has units of (W/cm)/(atom/b-cm). It must be emphasized that the sensitivity coefficients as defined are applicable only in relation to gamma production processes, and hence do not include the sensitivity to the gamma transport processes or changes in the physical location of the gamma producing interactions. Table 12 presents the sensitivity coefficients for water. A negligible amount of Boron was included in the calculation to ascertain the effect of Boron (as a control poison) on the response. At a maximum concentration of 1178 ppm, the change in the response was on the order of $1.43 \cdot 10^{-6}$ W/cm, hence the use of boron as a control poison will have a negligible effect on the response (with respect to gamma production). However, there will be an indirect effect on the response due to suppression and or redistribution of the neutron flux (and hence the magnitude and, possibly the location of the gamma sources). The exact nature of this effect, however, is beyond the scope of this study. Table 13 presents the sensitivity coefficients for gamma production in the fuel (UO_2). Again, Pu^{239} and Pu^{240} were included in negligible quantities to obtain the sensitivity coefficients. Utilizing the total sensitivity coefficient for each material (last column, Table 13) and the results of an ORIGEN burnup analysis at 1000 days irradiation (33,800 MWD/MTHM), the results in Table 15 indicate that the overall response due to fuel does not change

Table 12. Sensitivity Coefficient by Material
and Reaction for Water [W/cm]/(atom/b-cm)]

Reaction Material	(n, γ)	(n,n' γ)	Total
H	2.9520-01	-	2.9520-01
O	2.8079-04	-	2.8079-04
B ¹⁰	-	3.5634-02	3.5637-02

Table 13. Sensitivity Coefficient by Material
and reaction for fuel (UO₂)
 $\frac{W/cm}{atom/b-cm}$

Reaction Material	(n, γ)	(n,f)	(n,n' γ)	(Misc)	Total
O	1.7201-04	-	-	-	1.7201-04
U ²³⁵	1.7749+02	6.9545+02	3.6001-02	5.2827+00	8.7826+02
U ²³⁸	1.0617+01	2.3064-04	-	3.3962+00	1.4013+01
Pu ²³⁵	1.1010+03	1.7138+03	1.3615-02	6.9964+00	2.8218+03
Pu ²⁴⁰	2.8655+03	3.1991+00	5.3868-02	6.5579+00	2.8753+03

Table 14. Sensitivity Coefficient by Material
and Reaction for Stainless Steel (SS-316L)
 $\frac{W/cm}{atom/b-cm}$

Reaction	(n, γ)	(n,n' γ)	(Misc)	Total
Material				
Fe	1.2103	0.0425	0.1847	1.4375
Ni	2.6581	0.0	0.2069	2.8650
Mn	6.9266	0.0	0.1768	7.1034
Cr	1.7937	0.0	0.2564	2.0501
Mo	5.6942	0.0	0.6095	6.3037
Trace Elements (C,Si,P,S)	0.5565	0.0787	0.1298	0.7650

Table 15. Energy Deposition in the GT Due to Gamma Production in the Fuel as a Function of Burnup

Material	Energy Deposition (W/cm)	Energy Deposition (W/cm)
	Beginning of Life	End of Life
U ²³⁵	0.5353	0.1377
U ²³⁸	0.2797	0.2726
Pu ²³⁹	0.0	0.2936
Pu ²⁴⁰	0.0	0.1251
Total	0.8550	0.8290

appreciably as a function of the isotopic changes inherent in burnup. However, the isotopics of the fuel change dramatically as a function of burnup, and it is anticipated that the primary effect on the response will be via changes in the gamma transport processes (an effect not considered in this study). Table 14 presents the sensitivity coefficients for gamma production due to stainless steel (i.e., the gamma thermometer itself). Since, it is desired that the signal from the gamma thermometer, itself be as small as possible, the results in the last column of Table 14 indicate that a material with a high Fe concentration and low concentrations of Ni, Cr, etc., will result in the least amount of spurious gamma production.

The primary results of the transport analysis indicate that the majority (approximately 78%) of the energy deposition rate is due to neutrons induced reactions, and 22% due to fission product decay. A second result indicated is that approximately 95% of the gamma source originates within the instrumented fuel element and therefore the response will not be a strong function of the element's location in the core. The final results indicate that of the neutron induced gamma source, approximately 2% originates in the water, 83% in the fuel, and 15% within the thermometer itself. A side light to this result is that the contribution from the fuel remains essentially constant as a function of burnup.

IV. THERMAL HYDRAULIC ANALYSIS

In addition to the characterization of the radiation field in the vicinity of the gamma thermometer (GT), the response of the GT to changes in the thermal-hydraulic environment is also of interest. This is particularly true concerning the proposed dual-function mode of operation. Although the one-dimensional analytic calculations (discussed in Chapter II) established the theoretical feasibility of such a dual function, verification of the "robustness" of the signal to detailed geometric modeling as well as to the actual time-dependent fluid property changes must be established. To investigate the effects of coolant-related parameters on the gamma thermometer signal, a prototypic calculational model of the gamma thermometer, depicted in Fig. 14, was created. The thermal hydraulics code HEATING-5¹⁰ was used to calculate the spatial and time dependence of the gamma thermometer signal. The coolant parameters utilized were typical of the thermal hydraulic environment of a PWR fuel assembly (Table 1). Further, the analysis incorporated the volumetric heat source obtained via the radiation transport calculations. Temperature dependent material properties were utilized for each material; the data being extracted from the Nuclear Systems Materials Handbook.¹¹

The analyses considered the behavior of the GT signal for both normal reactor operating conditions, as well as the behavior during and subsequent to various reactor transients. The transients analyzed were: (1) a reactor scram (modeled as an instantaneous termination of the gamma source attributable to neutron-induced reactions), (2) an instantaneous loss of coolant accident (LOCA) (modeled as an instantaneous change in the external heat transfer coefficient from approximately 25,000 W/m²°C - which represents normal reactor core conditions -- to 124 W/m²°C - which represents saturated steam at 15.5 MPA and 315°C), (3) a combination of a reactor scram and LOCA, (4) a 10 s ramp LOCA, and (5) a 40 s ramp LOCA.

In analyzing the applicability of the gamma thermometer as a power level monitor, two characteristic parameters of the generic GT are of interest: the calibration of the device with respect to the Local Heat Generation Rate (LHGR), and the time constant of the instrument itself.

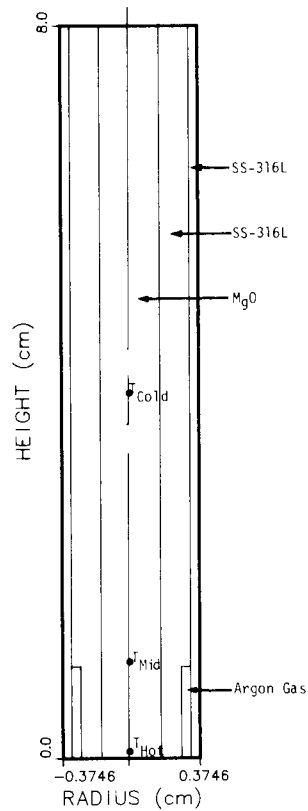


Fig. 14. Calculational Model of the Gamma Thermometer Used for Thermal Hydraulics Analysis.

The fundamental relationship between LHGR and the temperature differential between the hot and cold thermocouple junctions is postulated as [see Eq. (7)]:

$$(T_{\text{Hot}} - T_{\text{Cold}}) = a \cdot \text{LHGR} + b \quad (9)$$

where a is the proportionality constant relating the local heat generation rate to the temperature differential and b is, at this point, an arbitrary constant. It should be noted that a will depend on the fuel assembly geometry as well as on the gamma thermometer materials and geometry. Thus, the linear power inferred from the gamma thermometer signal can be expressed as

$$\text{LHGR}^* = \alpha \cdot (T_{\text{Hot}} - T_{\text{Cold}}) + \beta \quad (10)$$

Based on the radiation transport analysis presented in the previous section, and a series of static thermal-hydraulic calculations using the HEATING-5 computer code, the value of α was calculated to be 14.96 W/cm \cdot $^{\circ}$ C, and β was estimated as -55.19 W/cm. This relationship is depicted in Fig. 15 which presents the relationship between the local heat generation rate and the gamma thermometer response for a reactor core after 1000 full power days. It should be noted that the curve does not have a zero intercept (i.e., zero power does not imply zero ΔT). The primary reason behind this characteristic is the buildup and subsequent decay of fission products, which account for approximately 3% of the total thermal power generated. These gammas which contribute 3% of the total thermal power, however, contribute 22% of the gamma thermometer signal (see discussion in Chapter III). This result indicates that b in Eq. (9) and β in Eq. (10) are both functions of the reactor burnup (i.e., the amount of fission products present). However, since the fission product concentrations and consequently the fission product gamma source reach an asymptotic value after only a few full power days of operation,¹² β will essentially be a constant value except for a short time following initial reactor start-up (or restart). It should be noted, that for a cold clean

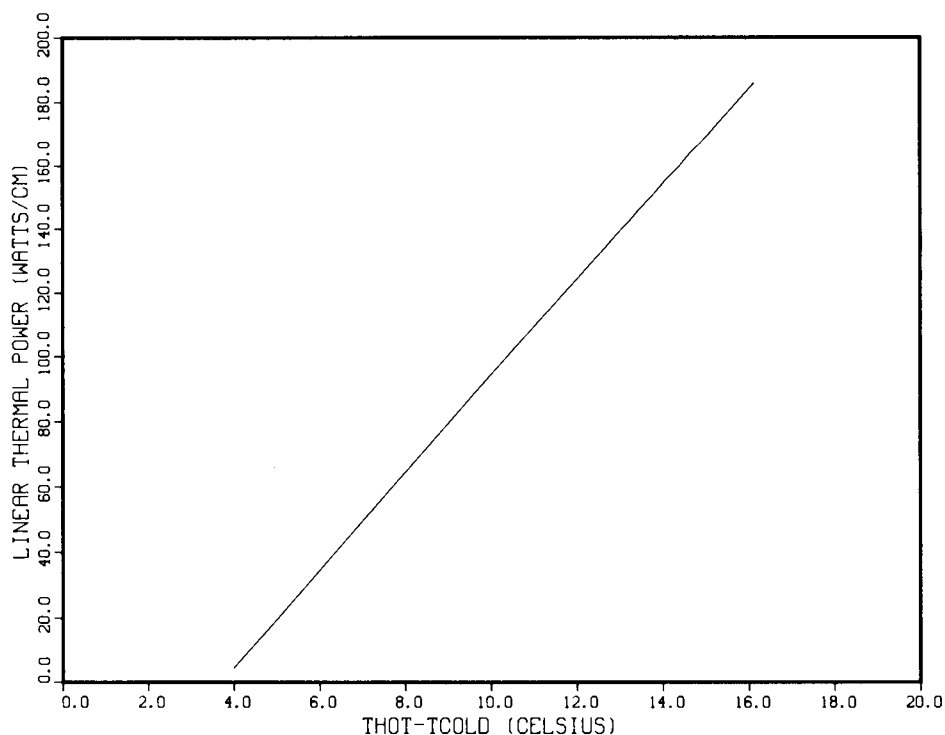


Fig. 15. Calibration Curves for the Power Level Indicator (33,800 MWD/MTHM Burnup).

core (i.e., no fission products), the initial value of β would be zero, and the resulting calibration curve would parallel the curve in Fig. 15. This result is due to the fact that α was found to be insensitive to burn-up and therefore remains constant as the fission product concentration approaches its asymptotic value.

The second characteristic of the gamma thermometer that affects its applicability as a power level monitor, is the time constant of the instrument itself. In Eq. (10), a relationship between the gamma thermometer signal ($T_{\text{Hot}} - T_{\text{Cold}}$) and the inferred LHGR* is given. Utilizing the values for α and β , and the differential temperature reading from a transient HEATING-5 calculation modeling an instantaneous reactor scram, a comparison of the actual and inferred LHGR (LHGR*) is shown in Fig. 16. The results presented in Fig. 16 indicate that the gamma thermometer attained the new power level reading approximately 40 s after the transient commenced. Assuming an exponential relationship, between ΔT and time, the thermocouple response time constant was estimated to be 0.0508 °C/s.

The results of the one-dimensional analytic calculations indicated that the power level indicator reading of the gamma thermometer ($T_{\text{Hot}} - T_{\text{Cold}}$) would be a strong function of the reactor power, but a relatively weak function of the thermal-hydraulic environment of the GT (principally, the external heat transfer coefficient). The preliminary indication is confirmed by these more detailed calculations. Figure 17 depicts the time-dependent power level indication (i.e., GT signal) as a result of an instantaneous reactor scram. The results indicate a factor of four change in the GT signal and therefore confirm the strong dependence of the GT signal on the power level as indicated by the one-dimensional analysis. The time dependence of the power level indication for an instantaneous LOCA (depicted in Fig. 18), after an initial transient effect, returns to the initial value. The initial transient behavior seen in Fig. 18 can be attributed to the different time constants for the two TC junctions within the gamma thermometer. This result is further exemplified in the power level indicator response to a 10 s ramp LOCA and 40 s ramp LOCA as shown in Figs. 19 and 20 respectively. The responses to the two ramp LOCA's display the same characteristic shape as does the response to the instantaneous

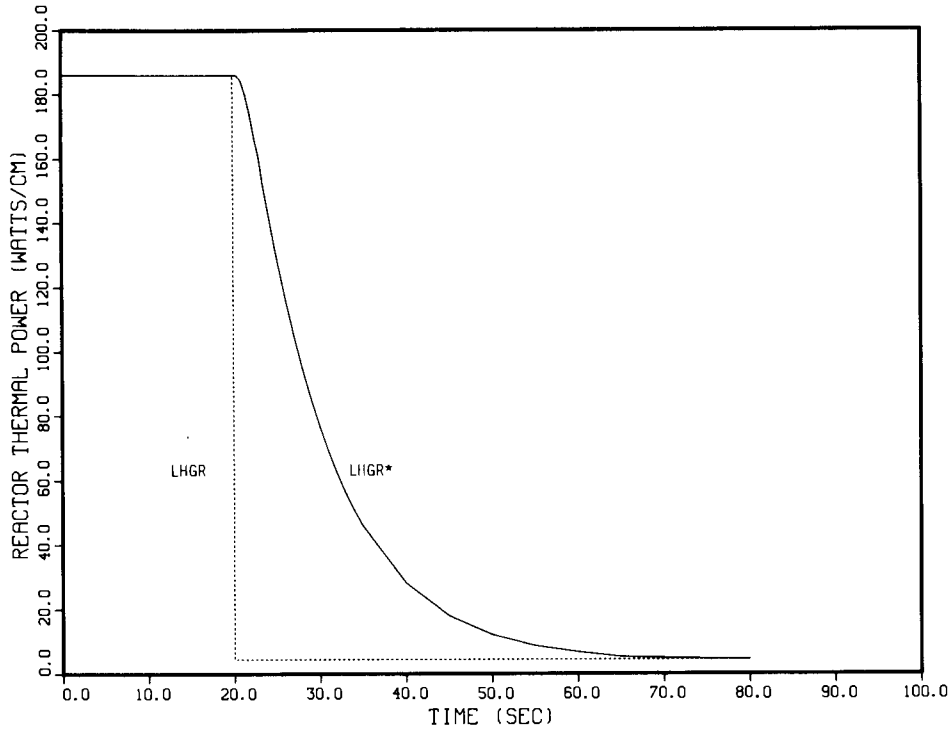


Fig. 16. Comparison of the Actual (LHGR) Versus Inferred Reactor (LHGR*) Thermal Power Subsequent to a Reactor Scram.

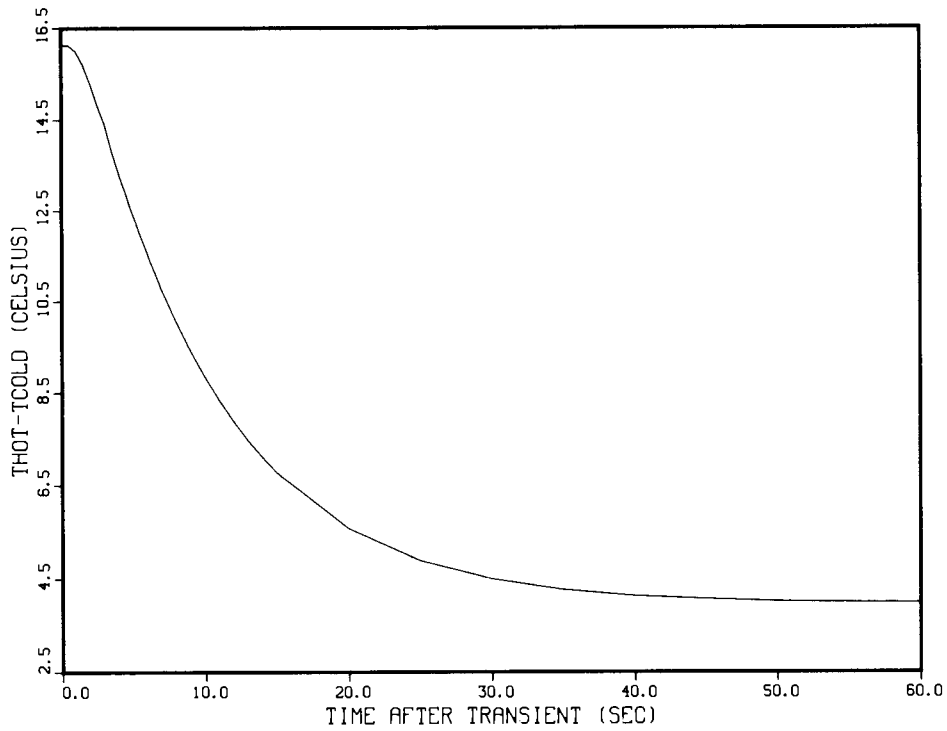


Fig. 17. Power Level Indicator Response Subsequent to an Instantaneous Reactor Scram.

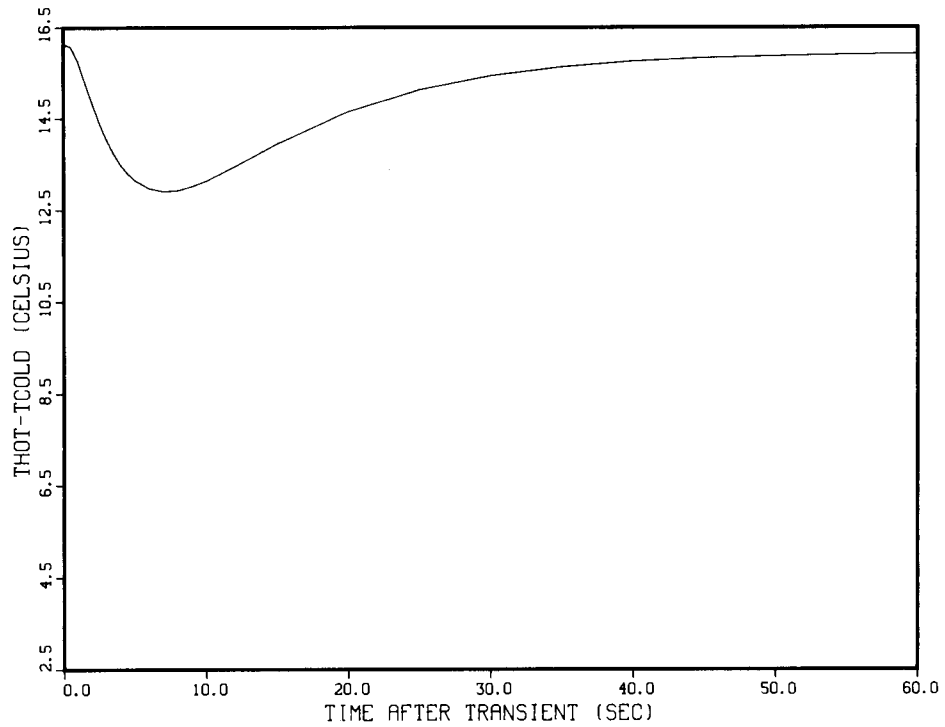


Fig. 18. Power Level Indicator Response Subsequent to an Instantaneous Loss of Coolant Accident (LOCA).

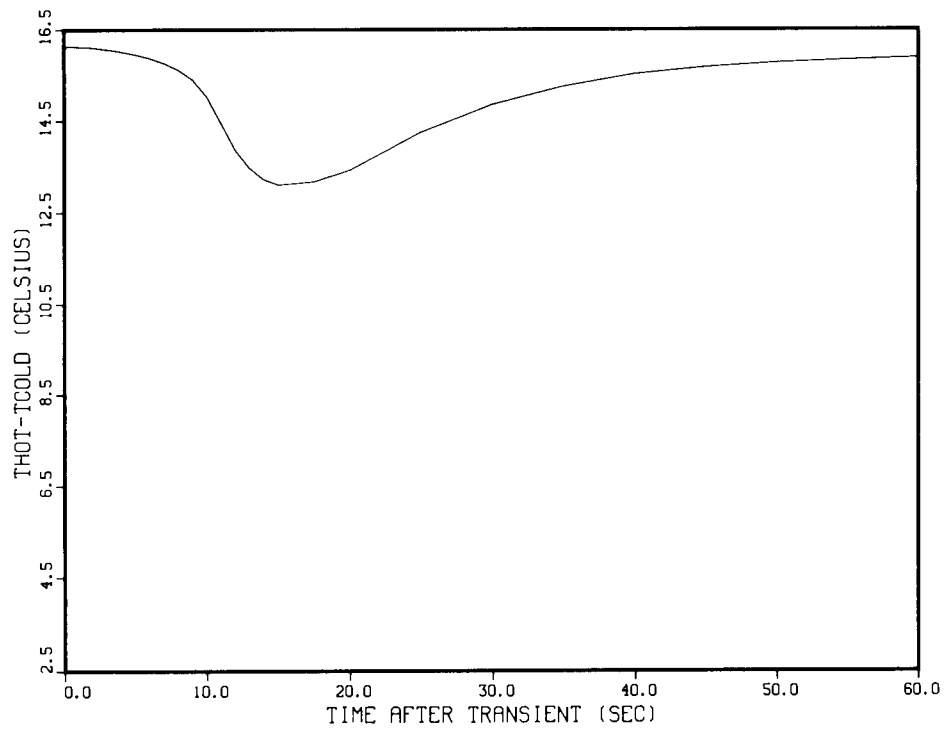


Fig. 19. Power Level Indicator Response Subsequent to a 10 s Ramp LOCA.

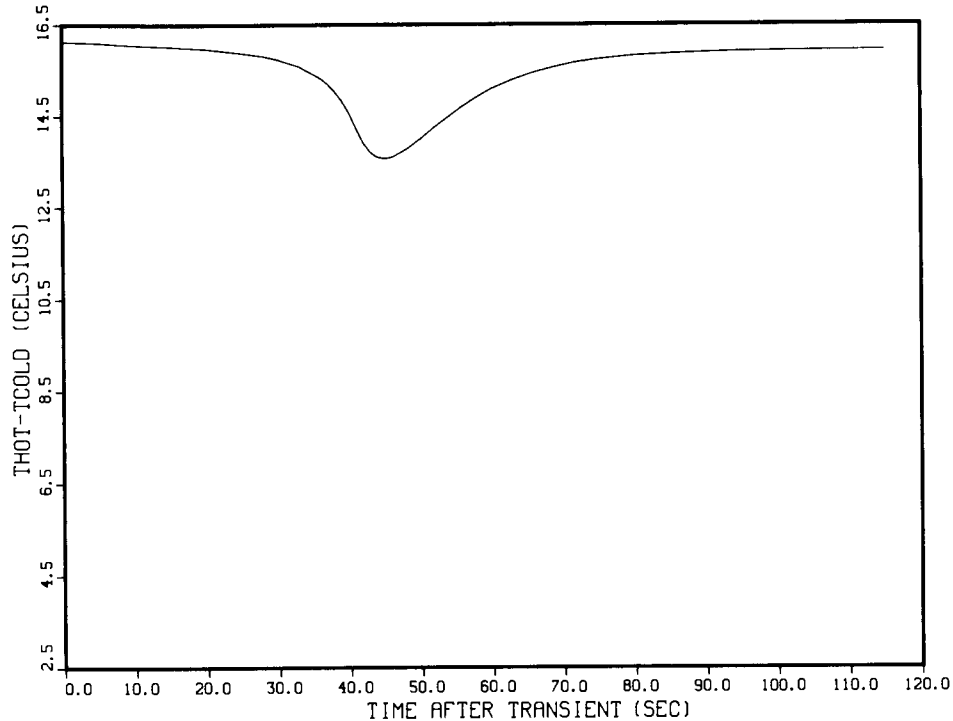


Fig. 20. Power Level Indicator Response Subsequent to 40 s Ramp LOCA.

LOCA except for a displacement by the amount of time it takes the ramp change to occur (responding to both the initiation of the ramp as well as its termination). As a final confirmation on the one-dimensional analytical results, a combination instantaneous reactor scram and LOCA was modeled in HEATING-5 with the powerlevel indicator reading shown in Fig. 21. In comparing Figs. 17 and 21, the results show no discernable difference (i.e., factor of four drop in both signals). This result indicates that the measured signal change is due primarily to the power level change and therefore is insensitive to the thermal-hydraulic environment outside the gamma thermometer.

The results of the one-dimensional analytical calculations also indicated that the fluid level indicator reading of the gamma thermometer ($T_{\text{Hot}} - T_{\text{Mid}} / (T_{\text{Mid}} - T_{\text{Cold}})$) would be a strong function of the thermal-hydraulic environment but independent of the reactor power. This result is confirmed in Figs. 22, 23 and 24 which represent the time dependent fluid level indication (i.e., GT signal) due to an instantaneous LOCA, a 10 s ramp LOCA, and a 40 s ramp LOCA respectively. In each case, the results show a

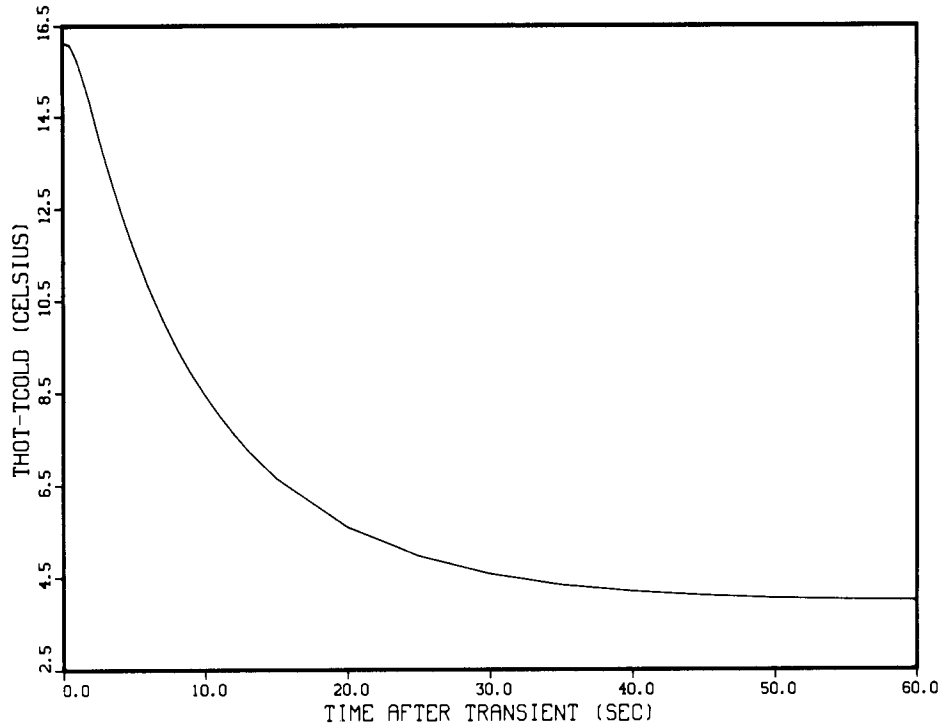


Fig. 21. Power Level Indicator Response Subsequent to a Combination Reactor Scram and LOCA.

decrease in the fluid level indication by a factor of two following the transient. As indicated by Figs. 23 and 24, the time dependent fluid level indication, analogous to the power level indication (see Figs. 19 and 20), is delayed due to the finite response time of the GT. The insensitivity of the fluid level indication to the reactor power is depicted in Fig. 25, which shows the gamma thermometer signal during and subsequent to an instantaneous reactor scram. The apparent noise in the signal is due to roundoff difficulties in the calculation — caused by the location choice for T_{Mid} . This can be rectified by a more judicious choice of T_{Mid} ; typically somewhat closer to the hot junction (see Fig. 14).

As in the case of the power level indication, the final confirmation of the one-dimensional analytical results for the fluid level indication is shown in Fig. 26 which represents the time dependent fluid level indication for a combined instantaneous reactor scram and LOCA. Analogous to the power level indication, the results indicate no discernable difference when comparing to the results of the fluid level indication for a LOCA alone [Fig. 22] (i.e., the same factor of two decrease in signal).

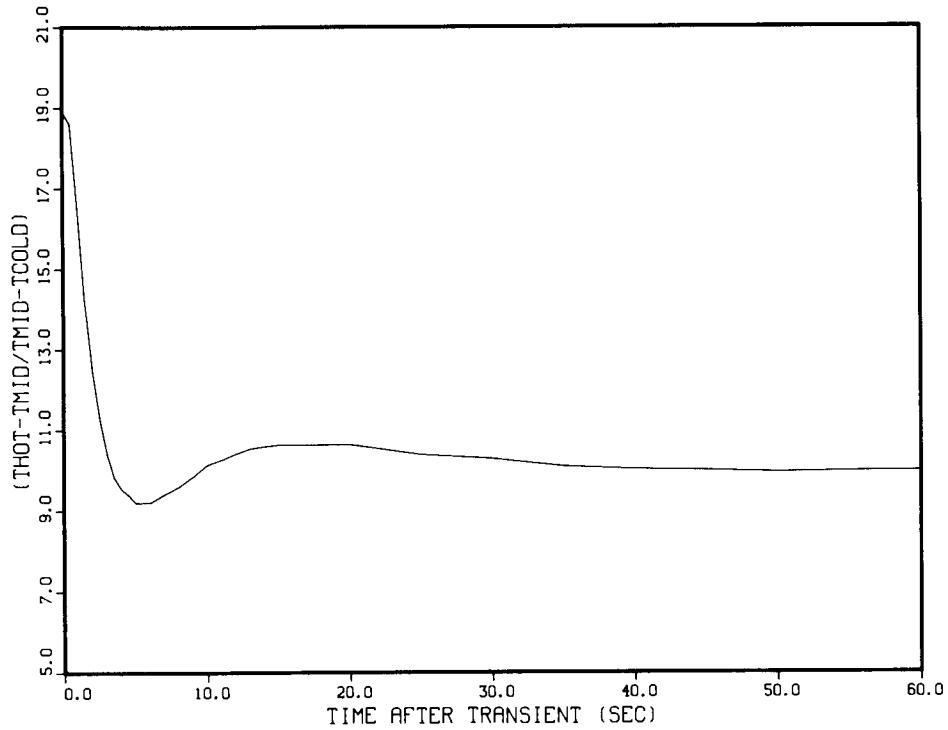


Fig. 22. Water Level Indicator Response Subsequent to an Instantaneous LOCA.

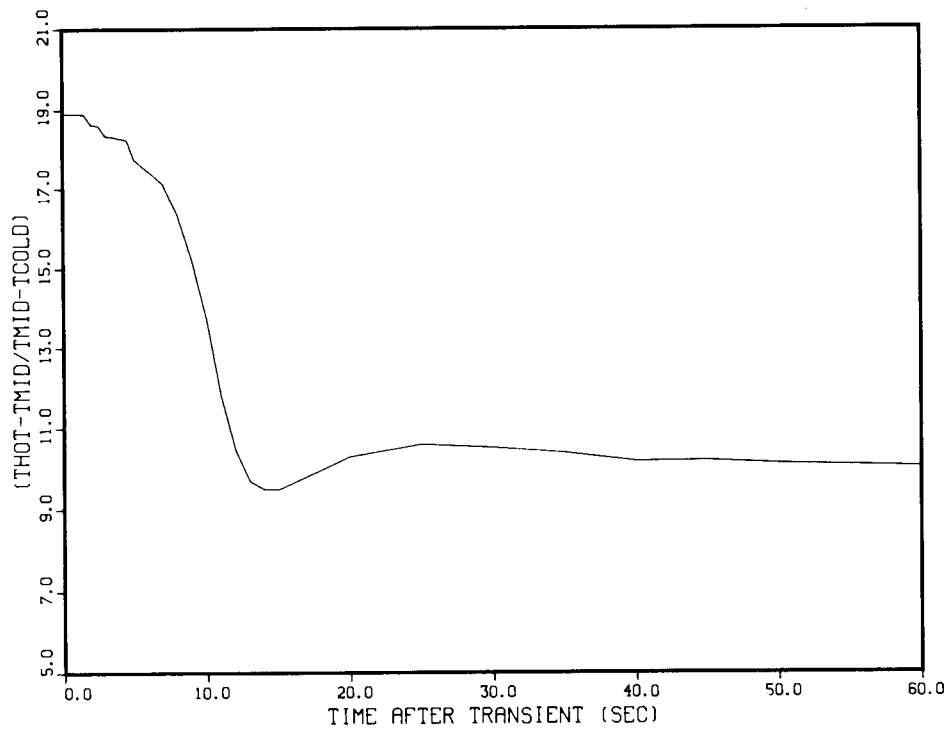


Fig. 23. Water Level Indicator Response Subsequent to a 10 s Ramp LOCA.

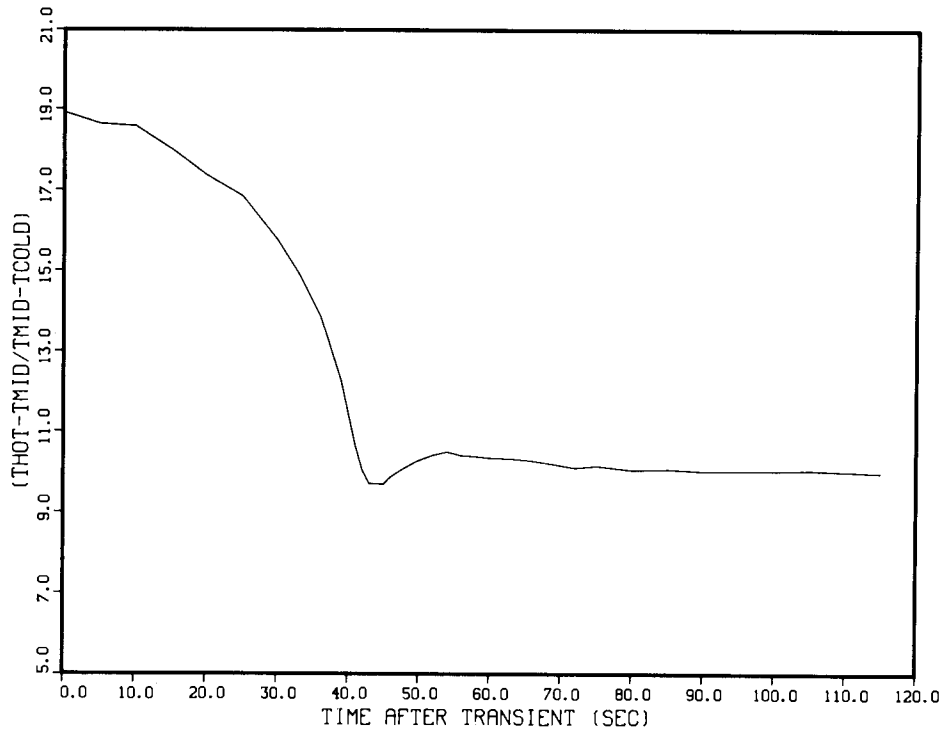


Fig. 24. Water Level Indicator Response Subsequent to a 40 s Ramp LOCA.

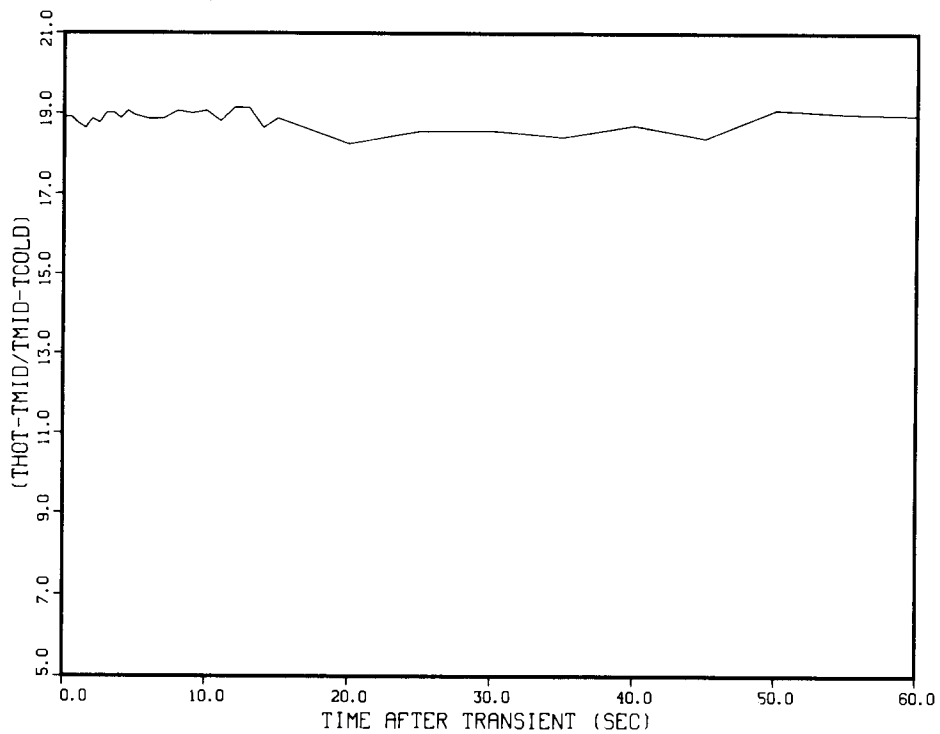


Fig. 25. Water Level Indicator Response Subsequent to an Instantaneous Reactor Scram.

This result indicates that the measured signal change is due almost entirely to the thermal-hydraulic environment external to the GT and is not influenced significantly by the power level.

In viewing the results presented in this section, the time dependent power level indication was shown to be a strong function of the reactor power for the case of a reactor scram (Fig. 17) yet insensitive to the thermal-hydraulic environment as seen in the time response to a LOCA (Fig. 18). In contrast, the fluid level indication was a strong function of the thermal-hydraulic environment as evinced in the time response to a LOCA (Fig. 22), but insensitive to the reactor power as seen in the time response to a reactor scram (Fig. 25).

The full potential of the gamma thermometer as a dual measuring device was confirmed in the results of the combination instantaneous reactor scram and LOCA. The power level indication (Fig. 21) and the fluid level indication (Fig. 26) both registered a drop in signal strength. However, the decreases associated with each measurement are virtually independent of each other as discussed above and correspond to those attributable to those calculated for single events. Therefore, the use of the GT as a dual measuring device is feasible since neither use will compromise the effectiveness with respect to the other function.

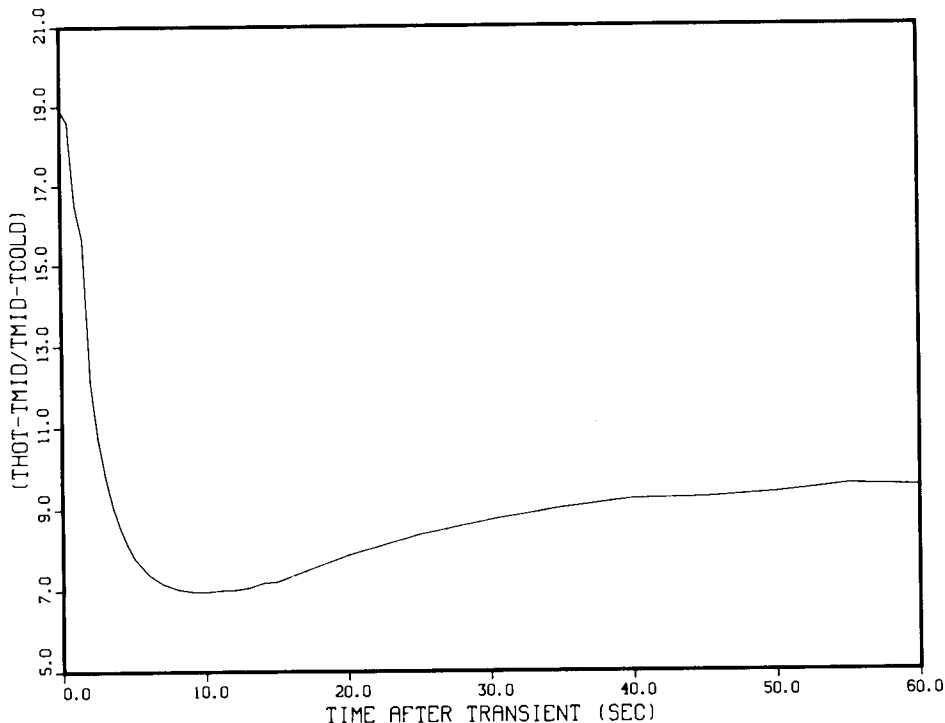


Fig. 26. Water Level Indicator Response Subsequent to a Combination Reactor Scram and LOCA.

V. CONCLUSIONS AND RECOMMENDATIONS

The initial contention that the gamma thermometer can be used as a dual function (power level and coolant level) measurement device has been upheld by the more detailed calculations described in this report. Moreover, the results presented here indicate that each function can be isolated to a large extent from the other. The signal utilized to indicate the power level is proportional to the LHGR, and is insensitive to the thermal-hydraulic environment. Conversely, the signal employed as a fluid level indicator is responsive to changes in the thermal-hydraulic environment, but not particularly sensitive to changes in reactor power. Thus, it should be possible to infer the state of the reactor even if both power level and the thermal-hydraulic environment change simultaneously (e.g. scram and LOCA).

The detailed characterization of the radiation field has established (for the specific fuel assembly and GT model considered) the geometrical location of the gamma sources relative to their importance to the GT signal as well as the materials and nuclear reactions contributing to the response. Specifically, the particles responsible for the GT signal are produced primarily in the instrumented assembly itself (~95%). Moreover, approximately 72% of the signal is produced by particles originating within the first three rows of fuel pins [68% of the neutron-induced gammas and 75% of the fission product gammas]. Hence the GT signal is very representative of the Local Heat Generation Rate (LHGR).

Of those gammas which contribute to the GT signal, 22% of the gammas are traceable to the decay of fission products within the fuel pins (at 33,800 MWD/MTHM burnup). Of the remaining 78% of the signal, 37% results from the prompt fission gammas and 41% is traceable to other neutron-induced reactions such as (n,γ) and $(n,n'\gamma)$. The total GT signal was also characterized by the region in which the gammas were produced: 83% originating in the fuel pins, 2% in the coolant, and 15% in the body of the gamma thermometer itself.

Based on the results of the transport analyses, the GT power level signal calibration will depend on burnup. Since the gammas from fission

products account for only 3% of the thermal power (reactor at full power) but 22% of the gamma thermometer signal at a burnup of 33,800 MWD/MTHM the calibration curve for the device will have a non-zero intercept in general. However, since the fission product gamma source reaches equilibrium rapidly (\sim a few full power days) such an effect represents only an initial transient for the start-up of the reactor (and possibly, a transient on re-start).

The thermal-hydraulic analyses described in this report have shown, in a preliminary sense, that the GT signal information can be utilized to measure both LHGR and the presence or absence of the reactor coolant at the GT active location. Although a very simplified model of the thermal hydraulic environment during a loss of coolant accident was employed, the results indicate that the fluid level application of the GT is viable. Moreover, the thermal-hydraulic analyses have indicated that the two functions, power-level and fluid-level indications, can be separated and distinguished. A reactor scram [decrease from 100% to 3% in thermal power] resulted in a reduction of the power level signal by a factor of 3.7. For this case however, no permanent change in the fluid level reading was apparent. On the other hand, the simulated LOCA [at power] resulted in the fluid level indication changing by a factor of 2.0 with no discernable change in the power level.

Although the results obtained in this study provide both encouragement and incentive to pursue the GT as a viable nuclear instrument, this study must be regarded as only a first step towards complete characterization of the device. In particular, the adequacy of the many approximations and assumptions that were necessary to perform this study must be validated. More specifically, the areas requiring further study or more detailed analysis are:

1. The effect of the two-dimensional discrete ordinates approximations. A three-dimensional Monte Carlo analysis is necessary to verify the overall LHGR to energy deposition rate relationship obtained in this study.
2. The effect of control rods within the instrumented assembly on the LHGR/GT relationship.

3. The time dependence of the GT signal as a function of burnup. Since the isotopics of the fuel change non-linearly with time, it is reasonable (in light of the sensitivity calculations presented in Chapter IV) that the GT calibration will also vary non-linearly as a function of fuel isotopics.
4. The influence of perturbations of the neutron field on the response of the GT. In this study, the sensitivities to the gamma production sources were determined for fixed locations. However, changes in the neutron field (e.g. due to changes in the boron concentration) will affect both the magnitude and the location of the gamma sources.
5. The effect of the very simplified model employed to model a LOCA for a PWR. Clearly, a more detailed description of the variation of the surface heat transfer coefficient, one which accounts for two-phase flow, film formation and thickness variations, etc., must be developed.



REFERENCES

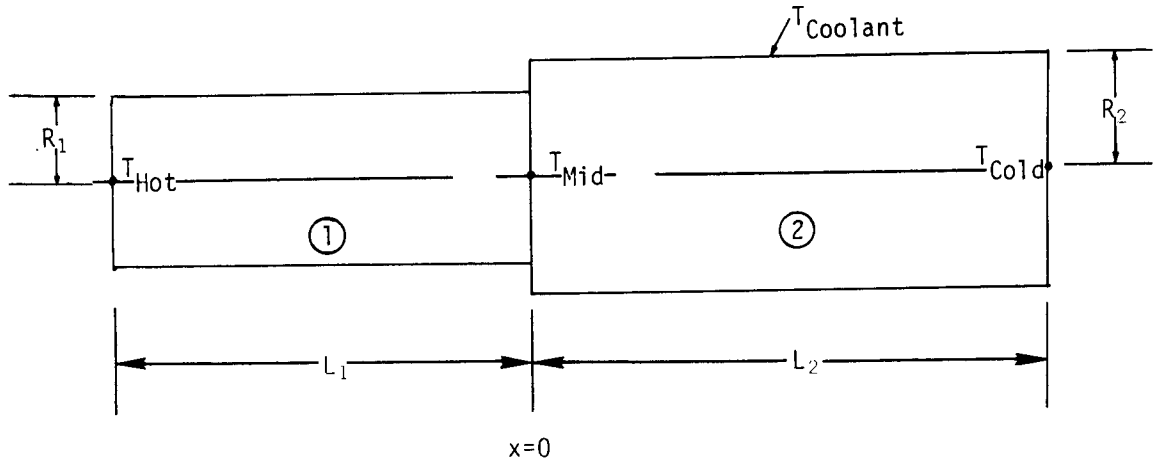
1. J. S. Stutheit, "Fast Response Gamma Thermometers," *Nuclear Instruments and Methods*, 63, 300-306 (1968).
2. R. H. Leye and R. D. Smith, "Gamma Thermometer Developments for Light Water Reactors," *IEEE Transactions on Nuclear Science*, NS-26, 934-942 (1979).
3. N. M. Greene, W. E. Ford, III, et al., "AMPX: A Modular Code System for Generating Coupled Multigroup Neutron-Gamma Libraries from ENDF/B," ORNL/TM-3706 (1976).
4. W. E. Ford, III, C. C. Webster, and R. M. Westfall, "A 218-Group Neutron Cross-Section Library in the AMPX Master Interface Format for Criticality Safety Studies," ORNL/CSD/TM-4 (1976).
5. W. A. Rhoades, D. B. Simpson, R. L. Childs, and W. W. Engle, "The DOT-IV Two-Dimensional, Discrete-Ordinates Transport Code with Space-Dependent Mesh and Quadrature," ORNL/TM-6529 (1978).
6. M. J. Bell, "ORIGEN - The ORNL Isotope Generation and Depletion Code," ORNL/TM-4629 (1973).
7. E. T. Tomlinson, R. L. Childs, and R. A. Lillie, "DOS Perturbation Modules DGRAD/VIP/TPERT," ORNL/CSD/TM-116 (1980).
8. D. E. Bartine, F. R. Mynatt, and E. M. Oblow, "SWANLAKE, A computer Code Utilizing ANISN Radiation Transport Calculations for Cross Section Sensitivity Analysis," ORNL/TM-3809 (1973).
9. W. E. Ford, III, Computer Science Division, ORNL, private communication (August 1980).
10. W. D. Turner, D. C. Elrod, and I. I. Simon-Tov, "HEATING-5 - An IBM 360 Heat Conduction Program," ORNL/CSD/TM-15 (1977).
11. *Nuclear Systems Materials Handbook*, TID-26666 Hanford Engineering Development Laboratory, Richland, Washington, Vol. 1.
12. M. M. El-Wakil, *Nuclear Heat Transport*, International Textbook Company (1971).



APPENDIX

Detailed Development of the Equations Used in the One-Dimensional
Thermal Hydraulic Analysis of the Gamma Thermometer





Let $\theta = T - T_{Cooolant}$ and $\frac{q}{k} = \text{constant}$

Define $m^2 = \frac{hP}{kA}$

Where $q = \text{volumetric heat generation rate, W/cm}^3$

$k = \text{thermal conductivity, W/cm } ^\circ\text{C}$

$h = \text{convective heat transfer coefficient, W/cm}^2 \text{ } ^\circ\text{C}$

$P = \text{perimeter exposed to convection, cm}$

$A = \text{cross sectional area, cm}^2$

$T_{Hot} = \text{hot thermocouple junction temperature, } ^\circ\text{C}$

$T_{CoId} = \text{Cold thermocouple junction temperature, } ^\circ\text{C}$

$T_{Cooolant} = \text{coolant temperature, } ^\circ\text{C}$

$T_{Mid} = \text{Interface temperature, } ^\circ\text{C}$

$L = \text{length, cm}$

$R = \text{radius, cm}$

General equation for region 1

$$\frac{d^2\theta}{dx^2} + \frac{q}{k} = 0$$

Integrating yields:

$$\frac{d\theta}{dx} = -\frac{q}{k}x + C_1$$

Integrating again yields:

$$\theta = \frac{-qx^2}{2k} + C_1x + C_2$$

General equation for region ②

$$\frac{d^2\theta}{dx^2} + \frac{q}{k} - \frac{hP}{kA} \theta = 0$$

or

$$\frac{d^2\theta}{dx^2} - m^2\theta = \frac{-q}{k}$$

Solve homogeneous equation

$$\frac{d^2\theta}{dx^2} - m^2\theta = 0$$

$$\theta_H = C_3e^{-mx} + C_4e^{mx}$$

Solve for particular solution

$$\frac{d^2\theta}{dx^2} - m^2\theta = \frac{q}{k}$$

Assume $\theta_p = \text{constant} = \psi$

Therefore $\theta''_p = 0$

$$\text{and } -m^2\psi = -\frac{q}{k}$$

Therefore $\theta_p = \frac{+q}{m^2k}$

Combine homogeneous and particular solutions

$$\theta = \theta_H + \theta_p = C_3e^{-mx} + C_4e^{mx} + \frac{q}{m^2k}$$

Take derivative

$$\frac{d\theta}{dx} = -C_3 m e^{-mx} + C_4 m e^{mx}$$

Boundary conditions:

$$\textcircled{1} \quad \frac{d\theta_1}{dx} = 0 \quad \text{at} \quad x = -L_1$$

$$\textcircled{2} \quad \frac{d\theta_2}{dx} = 0 \quad \text{at} \quad x = L_2$$

Interface conditions:

$$\textcircled{3} \quad \theta_1 = \theta_2 \quad \text{at} \quad x = 0$$

$$\textcircled{4} \quad -kA_1 \frac{d\theta_1}{dx} = -kA_2 \frac{d\theta_2}{dx} \quad \text{at} \quad x = 0$$

Apply boundary conditions

$$\left. \frac{d\theta_1}{dx} \right|_{x = -L_1} = 0 = \frac{-q}{k} (-L_1) + C_1$$

Therefore

$$C_1 = \frac{-qL_1}{k} \quad \text{and} \quad \theta_1 = \frac{-qx^2}{2k} - \frac{qL_1 x}{k} + C_2$$

$$\left. \frac{d\theta_2}{dx} \right|_{x = L_2} = 0 = -C_3 m e^{-mL_2} + C_4 m e^{mL_2}$$

Which yields

$$C_3 e^{-mL_2} = C_4 e^{mL_2}$$

Therefore

$$C_4 = C_3 e^{-2mL_2} \quad \text{and} \quad \theta_2 = C_3 \left[e^{-mx} + e^{-2mL_2} e^{mx} \right] + \frac{q}{m^2 k}$$

Apply interface conditions that

$$\theta_1 = \theta_2 \quad \text{at } x = 0$$

Which yields

$$\frac{-qx^2}{2k} - \frac{qL_1x}{k} + C_2 = C_3 \left[e^{-mx} + e^{-2mL_2} e^{mx} \right] + \frac{q}{m^2k}$$

Therefore

$$C_2 = C_3 \left[1 + e^{-2mL_2} \right] + \frac{q}{m^2k}$$

and the condition that

$$-kA_1 \frac{d\theta_1}{dx} = -kA_2 \frac{d\theta_2}{dx}$$

Which yields (at $x = 0$)

$$\frac{d\theta_1}{dx} = \frac{A_2}{A_1} \frac{d\theta_2}{dx} = \frac{\pi R_2^2}{\pi R_1^2} \frac{d\theta_2}{dx} = \frac{R_2^2}{R_1^2} \frac{d\theta_2}{dx}$$

$$\frac{-qx}{k} - \frac{qL_1}{k} = \frac{R_2^2}{R_1^2} C_3 \left[-me^{-mx} + me^{-2mL_2} e^{mx} \right]$$

Which further yields

$$\frac{-qL_1}{k} = \frac{-R_2^2 m}{R_1^2} C_3 \left[1 - e^{-2mL_2} \right]$$

Therefore

$$C_3 = \frac{\frac{qL_1 R_1^2}{km R_2^2}}{(1 - e^{-2mL_2})}$$

And consequently

$$C_2 = \frac{qL_1R_1^2}{kmR_2^2(1 + e^{-2mL_2})} + \frac{q}{m^2k}$$

Final Solutions:

Region ①

$$\theta_1 = \frac{-qx^2}{2k} - \frac{qL_1x}{k} + \frac{qL_1R_1^2}{kmR_2^2(1 + e^{-2mL_2})} + \frac{q}{m^2k}$$

Region ②

$$\theta_2 = \frac{qL_1R_1^2}{kmR_2^2} \frac{(e^{-mx} + e^{-2mL_2} e^{mx})}{(1 - e^{-2mL_2})} + \frac{q}{m^2k}$$

Therefore

At $-L_1$, $\theta_1 = \theta_{\text{Hot}}$, and

Therefore

$$\theta_{\text{Hot}} = \frac{qL_1^2}{2k} + \frac{qL_1R_1^2}{kmR_2^2} \frac{(1 + e^{-2mL_2})}{(1 - e^{-2mL_2})} + \frac{q}{m^2k} \quad (1)$$

At L_2 , $\theta_2 = \theta_{\text{Cold}}$

Therefore

$$\theta_{\text{Cold}} = \frac{\frac{2qL_1R_1^2}{kmR_2^2} e^{-mL_2}}{(1 - e^{-2mL_2})} + \frac{q}{m^2k} \quad (2)$$

Subtract Eq. (2) from Eq. (1)

$$(\theta_{\text{Hot}} - \theta_{\text{Cold}}) = (T_{\text{Hot}} - T_{\text{Coolant}}) - (T_{\text{Cold}} - T_{\text{Coolant}}) = (T_{\text{Hot}} - T_{\text{Cold}})$$

Therefore

$$(T_{\text{Hot}} - T_{\text{Cold}}) = \frac{qL_1^2}{2k} + \frac{qL_1R_1^2}{kmR_2^2} \left[\frac{(1 + e^{-2mL_2}) - 2e^{-mL_2}}{(1 - e^{-2mL_2})} \right] \quad (3)$$

Dividing the above equations yields

$$\frac{(T_{\text{Hot}} - T_{\text{Coolant}})}{(T_{\text{Cold}} - T_{\text{Coolant}})} = \frac{\frac{L_1^2}{2} (1 - e^{-2mL_2}) + \frac{L_1R_1^2}{mR_2^2} (1 + e^{-2mL_2}) + \frac{1}{m^2} (1 - e^{-2mL_2})}{\frac{2L_1R_1^2}{mR_2^2} e^{-mL_2} + \frac{1}{m^2} (1 - e^{-2mL_2})} \quad (4)$$

Evaluate either Eq. (1) or Eq. (2) at $x = 0$

and define $\theta_{\text{Mid}} = \theta|_{x=0}$

$$\theta_{\text{Mid}} = \frac{qL_1R_1^2}{kmR_2^2} \frac{(1 + e^{-2mL_2})}{(1 - e^{-2mL_2})} + \frac{q}{m^2k} \quad (5)$$

Subtracting Eq. (5) from Eq. (1) yields

$$(T_{\text{Hot}} - T_{\text{Mid}}) = \frac{qL_1^2}{2k} \quad (6)$$

And subtracting Eq. (2) from Eq. (5) yields

$$(T_{\text{Mid}} - T_{\text{Cold}}) = \frac{qL_1R_1^2}{kmR_2^2} \left[\frac{(1 + e^{-2mL_2}) - 2e^{-mL_2}}{(1 - e^{-2mL_2})} \right] \quad (7)$$

So that

$$\frac{(T_{\text{Hot}} - T_{\text{Mid}})}{(T_{\text{Mid}} - T_{\text{Cold}})} = \frac{\frac{mL_1 R_2^2}{2R_1^2} (1 - e^{-2mL_2})}{\left[(1 + e^{-2mL_2}) - 2e^{-mL_2} \right]} \quad (8)$$



INTERNAL DISTRIBUTION

- | | | | |
|--------|---------------------------|--------|------------------------------------|
| 1-2. | L. S. Abbott | 32. | W. A. Rhoades |
| 3. | R. L. Anderson | 33. | D. L. Selby |
| 4. | D. E. Bartine | 34. | R. L. Shepard |
| 5-9. | T. J. Burns | 35. | C. O. Slater |
| 10. | R. M. Carroll | 36. | D. B. Trauger |
| 11. | R. L. Childs | 37. | K. G. Turnage |
| 12. | W. W. Engle, Jr. | 38. | M. L. Williams |
| 13. | G. F. Flanagan | 39. | A. Zucker |
| 14. | H. Goldstein (Consultant) | 40. | P. Greebler (Consultant) |
| 15. | W. O. Harms | 41. | H. J. C. Kouts (Consultant) |
| 16. | J. L. Horton | 42. | W. B. Lowenstein (Consultant) |
| 17. | D. T. Ingersoll | 43. | R. Wilson (Consultant) |
| 18-22. | J. O. Johnson | 44-45. | Central Research Library |
| 23. | F. B. K. Kam | 46. | Y-12 Document Reference
Section |
| 24. | R. K. Kibbe | 47-48. | Laboratory Records Dept. |
| 25-29. | F. C. Maienschein | 49. | Laboratory Records, ORNL, RC |
| 30. | J. F. Mincey | 50. | ORNL Patent Office |
| 31. | F. J. Muckenthaler | | |

EXTERNAL DISTRIBUTION

- | | | | |
|-----|---|-----|---|
| 51. | Mr. H. B. Adams, Projects Mgr.
Energy Demonstrations & Tech.
Tennessee Valley Authority
1300 Commerce Union Bank Bldg.
Chattanooga, TN 37405 | 55. | Edward Fuller, Safety and
Licensing Coordinator
Engineering Division
Project Management Corp.
P.O. Box U
Oak Ridge, TN 37830 |
| 52. | J. W. Bennett, Director
Fuels and Components Division
U.S. Dept. of Energy
Washington, D. C. 20545 | 56. | Jerry Griffith, Director
Office of Light Water Reactors
U.S. Dept. of Energy
Washington, D. C. 20545 |
| 53. | Mr. Dale Bradshaw
Power Planning Advisor
Division of Power Mgr. Office
Tennessee Valley Authority
1300 Commerce Union Bank Bldg.
Chattanooga, TN 37405 | 57. | Richard Kanazawa
Electric Power Research
Institute
3412 Hillview Ave.
P.O. Box 10412
Palo Alto, Calif. 94304 |
| 54. | Fredrick W. Buckman, Director
Nuclear Activities
Consumer's Power Co.
212 W. Michigan Ave.
Jackson, Mich. 49201 | 58. | Robert Kubik, Program Mgr.
Nuclear Safety Analysis Ctr.
3412 Hillview Ave.
P.O. Box 10412
Palo Alto, Calif. 94303 |

59. Peter Morris
Executive Vice President
Scandpower Inc.
Suite B2, Triangle Towers
4853 Cordell Ave.
Bethesda, MD 20014
60. W. O. Parker, Jr.
Vice President
Duke Power Co.
Steam Production Dept.
422 S. Church St.
Charlotte, N. C. 28242
61. Office of the Assistant Manager
for Energy Research and
Development
DOE, ORO
Oak Ridge, TN 37830
- 62-63. Technical Information Center
U.S. Department of Energy
Oak Ridge, TN 37830